ÇUKUROVA UNIVERSITY
INSTITUTE OF NATURAL AND APPLIED SCIENCES

MSc THESIS

Umut ERCAN

MODELLING OF CYLINDRICAL HELICAL SIEVE

DEPARTMENT OF MECHANICAL ENGINEERING

ADANA, 2012

ÇUKUROVA UNIVERSITY
INSTITUTE OF NATURAL AND APPLIED SCIENCES

MODELLING OF CYLINDRICAL HELICAL SIEVE

Umut ERCAN

MSc THESIS

DEPARTMENT OF MECHANICAL ENGINEERING

We certify that the thesis titled above was reviewed and approved for the award of degree of the Master of Science by the board of jury on.

……..... …….....	……..	…….....
Prof. Dr. İbrahim Deniz AKÇALI	Prof. Dr. Vebil YILDIRIM	Assoc. Prof. Dr. Ahmet İNCE
SUPERVISOR	MEMBER	MEMBER

This MSc Thesis is written at the Department of Institute of Natural And Applied Sciences of Çukurova University.
Registration Number:

Prof. Dr. Director Selahattin SERİN
Institute of Natural and Applied Sciences

This study was supported by Scientific Research Projects office of Çukurova University (BAP) under grant No. MMF2011YL12

ABSTRACT

MSc THESIS

MODELLING OF CYLINDRICAL HELICAL SIEVE

Umut ERCAN

ÇUKUROVA UNIVERSITY
INSTITUTE OF NATURAL AND APPLIED SCIENCES
DEPARTMENT OF MECHANICAL ENGINEERING

Supervisor : Prof. Dr. İbrahim Deniz AKÇALI
Year: 2012, Pages: 71
Jury : Prof. Dr. Vebil YILDIRIM
: Assoc. Prof. Dr. Ahmet İNCE

In this study, the system called cylindrical helical sieve has been undertaken with the purpose of estimating its performance. The method of analysis has been analytical. The sieve has been modeled mathematically with respect to its flow-rate, energy use, efficiency and effectiveness. In another part of the study, an experimental model of the sieve has been set up for measuring flow-rate, energy consumed, effectiveness and efficiency for comparison purposes. In the end, a set of new semi-empirical relationships has been obtained to stand for the performance of the machine, which is supposed to optimize the use of resources.

Key Words: Cylindrical sieve**,** Granular material, Mathematical model, Design algorithm, Screening conditions.

ÖZ

YÜKSEK LİSANS TEZİ

SİLİNDİRİK HELİSEL ELEĞİN MODELLENMESİ

Umut ERCAN

ÇUKUROVA ÜNİVERSİTESİ
FEN BİLİMLERİ ENSTİTÜSÜ
MAKİNE MÜHENDİSLİĞİ ANABİLİM DALI

Danışman : Prof. Dr. İbrahim Deniz AKÇALI
Yıl: 2012, Sayfa: 71
Jüri : Prof. Dr. Vebil YILDIRIM
: Assoc. Prof. Dr. Ahmet İNCE

Bu çalışmada, silindirik helisel elek adı verilen sistemin performansı modellenmiştir. Analiz yöntemi analitik metottur. Eleğin matematik modellenmesi, besleme hızı, verimlilik ve etkili enerji kullanımını içermektedir. Çalışmanın diğer bir noktasında ise, karşılaştırma amaçları için eleğin deneysel bir modeli kurulmuş olup besleme hızı, verimlilik, tüketilen enerji etkin kullanımı laboratuar koşullarında ölçülmüştür. Araştırmanın sonunda, yeni bir makinenin performansını anlatan kuramsal ve deneysel parametrelerin değerleri saptanmıştır.

Anahtar Kelimeler: Silindirik Elek, Taneli Ürünler, Matematik Model, Tasarım Algoritması, Eleme Koşulları.

ACKNOWLEDGMENTS

I want to thank to my thesis advisor, Prof. Dr. İbrahim Deniz Akçalı, for his guidance, support throughout my research. He has been full of ideas, enthusiasm and always motivating and I enjoyed working with him a lot. I also want to thank, to my colleagues and my family, especially my mother Kadriye ERCAN, my father Yusuf ERCAN, my sister Bahar ERCAN for their encouragement and support. I want to thank to my beloved friend Beyza KÖSE for her patience, inspiration unending love and support. I would like to thank Prof. Dr. Emin Güzel and Assoc. Prof. Dr. Ahmet İnce for their support and help.

I also appreciate the support given by MACTİMARUM Research and Application Center, Laboratory of Agricultural Machinery Department, Cukurova University.

CONTENTS **PAGE**

LIST OF TABLES **PAGE**

LIST OF FIGURES **PAGE**

NOMENCLATURE

c	sheet metal thickness (m)
dm	infinitesimal mass of layer per unit length (kg/m)
dm/dt	mass flow rate along cylinder axis (kg/s)
D_d	diameter of helicoid piece (m)
D_d'	external diameter of ring (m)
D_i'	internal diameter of ring (m)
e	thickness of layer (m)
E	energy consume (kWs)
F_{net}	net force (N)
g	gravitational acceleration (m/s^2)
G	power (W)
h	pitch (m)
h	layer thickness (-)
K, B	small and big size group (g)
l_a, l_b	hole width and length (m)
n	number of layer (-)
r	cylinder radius (m)
$\ddot{S}$	acceleration of item (m/s^2)
$\ddot{S}_c, \ddot{S}_h$	accelerations along circular and helical paths (m/s^2)
T	total mass (g)
T_o	moment about cylinder axis per unit length (Nm/m)
V_s	relative velocity along helical path (m/s)
V_z	transport velocity of granular material along the cylinder axis (m/s)
V_θ	tangential cylinder velocity (m/s)
y	co-ordinate axis along gravitational acceleration (m)
z	co-ordinate axis along the cylinder axis (m)
ω	angular velocity (r/s)
a	width of helicoid piece (m)

α_*	angles which the single item starts sliding motion (^{o})
α_{*c}	angle at which sliding occurs along circular paths (^{o})
α_{*h}	angle at which sliding occurs along helical paths (^{o})
β	equilibrium angle (r)
β_c , β_h	equilibrium angles for motion along circular, helical paths (r)
ρ	density of granular material (kg/m^3)
μ_d	coefficient of friction between item and cylinder surface (-)
μ_h	coefficient of friction between item and helicoid surface (-)
ψ, ψ'	helix angle and its complementary (^{o})
η_K , η_B	small and big size efficiency
η	overall efficiency

1. INTRODUCTION

Sorting is the separation of foodstuff into categories on the basis of a measurable physical property (Fellows, 2000). Like cleaning, sorting should be employed as early as possible to ensure a uniform product for subsequent processing. The main objective of sorting is to provide uniformity over the food raw material, which is often said to be preferred by consumers. Other advantages of sorting is to secure product standardization, efficiency in subsequent processing of raw foodstuff and to make it possible to express other characteristics by means of the fundamental physical parameter.

Shape sorting is useful in case where the granular materials are contaminated with particles of similar size and weight. The principal disc or cylinders with accurately shaped indentations will pick up seeds of the correct shape when rotated through the stock, while other shapes will remain in the feed.

Size sorting, which is the separation of solids into two or more fractions on the basis of differences in size, is one of the frequently used processes in the preparing of food. Sorting into size categories requires different type of screens.

Colour sorting method can also be used to separate materials which are to be processed separately, such as red and green tomatoes. It is feasible to use transmittance as a basis for sorting, although as most foods are completely opaque, very few opportunities are available. The principle has been used for sorting cherries with and without stones and for the internal examination, or candling of eggs.

Grading is classification on the basis of quality incorporating commercial value, end use and official standards and hence requires that some judgments on the acceptability of the food is made, based on simultaneous assessment of several properties, followed by separation into quality categories (Grandison, 2006). Appropriate inspection belts or conveyors are designed to present the whole surface to the operator. There is much interest in the development of rapid, nondestructive methods of assessing the quality of foods, which could be applied to the grading and sorting of foods, the potential application of advanced optical techniques to give information on both surface and internal properties of fruits, including textural and

chemical properties. This could permit classification of fruit in terms of maturity, firmness or the presence of defects, or even more specifically, the noninvasive detection of chlorophyll, sugar and acid levels. Another promising approach is the use of sonic techniques to measure the texture of fruits and vegetables. Similar applications of X-rays, lasers, infrared rays and microwaves have also been studied.

Computer vision has been used for such tasks as shape classification, defect detection, quality grading and variety classification.

The objective of this thesis is to investigate analytically the sorting function of a system called cylindrical helical sieve. Here, the motion of granular material has been modeled in cylindrical medium rotated at a constant angular velocity on the basis of single item and of multilayer of granular material guided along circular, helical and combined paths. Efficiency, torque, power and energy experiments have been done. Experimental and theoretical results have been compared with each other. Finally, the optimum operating conditions of the cylindrical helical sieve have been determined.

2. PREVIOUS STUDIES

A wide range of mechanical separation equipment is used in food processing. Some basic equipment, such as vibrating screens, optical sorting, colour sorting, and, are adapted from the food process industry. Fundamental food processing research is focused on the physical and engineering properties of foods, which are required in the quantitative design of food processes, food processing equipment.

The type of driving mechanisms in relation to performance of vibrating screen has been the subject of many studies. For instance, in one of them (Tan & Harrison, 1987) influence of several different planar and spatial drive mechanisms on the screening efficiency has been worked out to obtain optimum performance in terms of the so called screening index. Yet in another work (Shen et al., 2009), a novel vibration sieve mechanism using a parallel mechanism has been proposed. Here optimum design based on structure, kinematic analysis and motion simulation has been demonstrated. The motion of granular material has also been analyzed in another work (Hongchang et al., 2011) with respect to a performance parameter called throwing index .In this analysis the most suitable value of throwing index has been found corresponding to the best performance of vibration screen.

The vibrating screen has found extensive applications in many different industries. For instance, in coal processing in mining science, vibrating screens have been taken into account from the standpoint of their “ideal motion” with the purpose of improving processing capacity and efficiency within the frame work of computer models (He & Liu, 2009).Vibrating screen with variable elliptical trace has been proposed resultantly. Another work for computer model of sieves’ vibrations analysis has been done in civil engineering construction bulk material screening using an algorithm based on the so-called false-position method (Stoicovici et al., 2009).

There have been some works related to the vibratory motion of the granular material using the so-called discrete element method. For instance, screening phenomena has been analyzed in another mechanical environment called vertical tumbling cylinder (Alkhaldi & Eberhard, 2006), whereby the concept of discrete element method (DEM) that considers the motion of each single particle individually

has been applied. A numerical study of the motion particulates along a circularly vibrating screen deck has been done using the three dimensional Discrete Element Method (DEM) (Lala et al., 2011). Here the effect of vibration amplitude, throwing index and screen deck inclination angle on the screening process has been determined for optimizing screen separator designs.

Optimization of vibrating screen has also been carried out using commercial software such as Matlab (Shuang & Nian-qin, 2010). In this study, on the basis of basic demand for vibration screen with high productivity, the mathematical model with maximum efficiency targets has been established while premising the screening productivity, and the optimization system.

This study point out that changing the position of components, although the all loads and all other dimensions remain the same; can have serious implication on the fatigue life of a component. Fatigue failure of deck support beams on a vibrating screen was surveyed by Jacques Steyn (Steyn, 1995).

Another study is dynamic design theory and application of large vibrating screen was design by Zhao Yue-min et al. (Zhao et all. 2009). They have used Finite Element Method (FEM) to analyze dynamic characteristic of large vibrating screen with hyperstatic net-beam structure. The structural size of stiffeners on the side plate was optimized under multiple frequencies constraints and an adaptive optimization criterion was given.

There are several studies in the literature that focus up on vibrating screen for maximization. For instance, research on dynamic characteristics of elliptical vibrating screen has been undertaken by utilizing finite element software ANSYS to carry on modal analysis and dynamic stress analysis of elliptical vibrating screen, and finds out the dynamic stress distribution and modal parameters (Zhongjun et all. 2010). Another study is parameters optimum design for linear vibrating screen in which mathematical model of linear vibrating screen with the pursuit of minimum power consumption per productive has been established using MATLAB software (Yan et all. 2010).

There are various systems utilizing image processing techniques. Computer vision systems have been used increasingly in industry for inspection and evaluation

purposes as they can provide rapid, economic, hygienic, consistent and objective assessment. However, difficulties still exist, evident from the relatively slow commercial uptake of computer vision technology in all sectors (Ata et all. 2005) For instance, colour recognition using fiber optic cabled sensors interfaced with robot controller and Programmable Logic Controller (PLC) in robotics application has been discussed (Brosnan, & Sun 2002).The aim of this research work is to recognize colour by pin point detection and sorting of object specimens with respect to their colour attributes, which includes hue, saturation and luminance level. Another study is inspection and grading of agricultural and food products by computer vision systems-a review. This study focuses on the progress of computer vision in the agricultural and food industry then identifies areas for further research and wider application of the technique. According to the Guang-rong L.,(Guang-rong 2010) color of rice is an important indicator of rice grade; this article has provided an objective and accurate way to inspect the rice color based on image processing technique . It has been shown that the application of two popular kinds of color model, Red, Green, Blue (RGB) model and H (hue), S (color saturation) and I (brightness) HSI model is feasible, in the rice color inspection. Computer vision has been used for such tasks as shape classification, defect detection, quality grading and variety classification.

Including the inspection of quality and grading of fruit and vegetable, non-destructive method of inspection has found applications in the agricultural and food industry. One study (Narendra & Hareesh, 2010) reviews the progress of computer vision in the agricultural and food field then explores different possible areas of research having a wider scope to enhance the existing algorithms to meet the today's challenges. Another study (Brosnan & Sun, 2004) has reported the recent developments and applications of image analysis in the food industry, the basic concepts and technologies associated with computer vision.

Grading method has been applied to Jonagold apples. Several images covering the whole surface of the fruits were acquired thanks to a prototype grading machine. Each blob was then characterized by 15 parameters: five for the colour, four for the shape, five for the texture and only one for its position. These images

were then segmented and the features of the defects were extracted. The prior step is the images acquisition, which was performed by Charge Coupled Device (CCD) cameras during the motion of the fruit on an adapted commercial machine. It was followed by a first segmentation to locate the fruits on the background and a second one to find the possible defects. Once the defects were located, they were characterized by a set of features including colour, shape, texture descriptors as well as the distance of the defects to the nearest calyx or stemend. The correct classification rate of Jonagold apples was of 73% (Unay & Gosselin 2004). In view of the lower efficiency despite the increasing number of parameter it is understood that in order to get better results, wavelength process could be offered to get better results.

Through the latest NIR (Near Infra Red) technology, packhouses can now sort their produce not just by size and color, but by indicators of produce taste. This is done without damaging produce as no mechanical mechanism touches the individual fruit. Brix is a measure of the percent of solids in a given weight of plant juice. It is often expressed as equaling the pounds of sucrose, fructose, vitamins, minerals, amino acids, proteins and other solids in one hundred pounds of a particular plant juice (Compact sorter).

The objective of this thesis is to investigate analytically the sorting function of a system called cylindrical helical sieve. Here, the motion of granular material has been modeled in cylindrical medium rotated at a constant angular velocity on the basis of single item and of multilayer of granular material guided along circular, helical and combined paths. Efficiency, torque, power and energy experiments have been done. Experimental and theoretical results have been compared with each other. Finally the effectiveness of the sorting system has been explained.

3. MATERIALS AND METHOD

In this study, firstly operation of sieve machine has been described. The sieve has been modeled mathematically with respect to its mass flowrate, energy use, efficiency and effectiveness. The mathematical model has been transformed into design algorithm. Finally, efficiency, mass flow rate, energy consumption and torque experiments have been done. Materials used in experiments have been characterized. Experiment material has been identified. The substance of this section is presented in two categories. One of them is the theoretical approach applied to the sieve machine and the other is the experimental approach to prefer it's perform.

3.1. Theoretical Approach

In theoretical approach, the sorting system called helical cylindrical sieve is described briefly. Then single – layer and multi – layer theories will be developed for the modeling of the system.

3.1.1. Cylindrical Helical Sieve System

The system shown in Figure 3.1 consists of two fundamental parts. One of these is the feeder and the other is cylindrical helical sieve. There are two sided brushes which are placed in parallel with the axis of the cylinder. These brushes are utilized to prevent blockage of the sieve holes. On the other hand, power consumption is supposed to increase because of to brushes. Power is provided by the electrical motor, and is transferred to the shaft of cylindrical sieve by belt-pulley system. As the cylinder rotates about its axis, the gate of the feeder is vibrated at the same time through a cylindrical cam mechanism to start the flow of the agriculture material into the sieve. Underneath the cylindrical sieve there exists a box for collecting the small-size material as well as another box for collecting big size material from the end of the sieve.

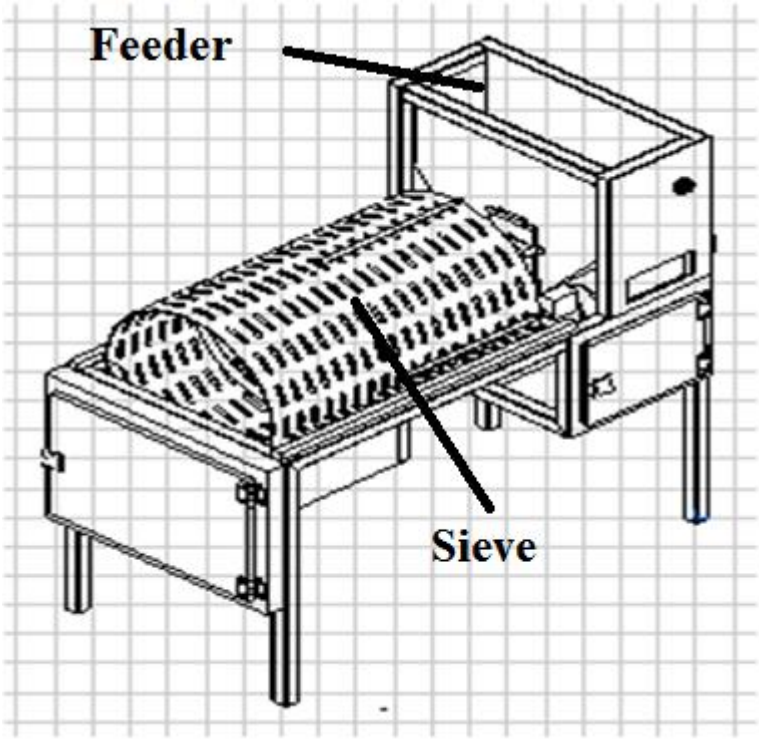

Figure 3.1. Cylindrical Helical Sieve

From the end of the cylinder, large- size material is collected. Besides, there is a technical feature of the feeder gate which allows the machine to operate at different flow rates.

In cylindrical sieve, which contains a helix wrapped to internal surfaces, the behavior of product will be examined while the sieve is rotating at a constant angular velocity. Three main forces direct the product inside the sieve medium: Centrifugal force due to the rotation of cylinder, product weight due to the gravity and friction forces between the product and the cylinder surfaces. Product will start to climb up to a certain height under the effect of centrifugal and friction forces and slide down back because of gravity.

3.1.2. Single Layer Theory

The motion of granular material in the cylindrical sieve, which contains helices wrapped onto internal surfaces, will be analyzed while the sieve is rotating at

a constant angular velocity. The study will be carried out basically in two steps: In the first step, the motion of a single item will be investigated. In the second step, the motion of granular material layer as a group will be studied. Here, it will be assumed that the granular material covers the internal surface of the cylinder continuously in the form of a single layer.

Three main forces which govern the motion of the material inside the sieve medium are the centrifugal force on the material resulting from the rotation of cylinder, material weight due to the gravitational acceleration and friction forces between the single granular material and the interacting surfaces. Granular material (one by one or in groups) will be carried by the rotating cylinder to a certain height under the effect of centrifugal and friction forces, and then will slide downwards from that height because of gravity.

Now, mathematical theory of the motion of granular material will be presented according to paths followed by either a single item or as a layer:

3.1.2.1. The Motion of one Single Item along a Circular Path

One of the paths along which a single item is supposed to move is a circular arc on the internal surface of a cylinder with radius r, which is rotated with angular velocity ω. Referring to Fig. 3.2, application of Newton's Second Law will lead to the following expression for the acceleration of the item:

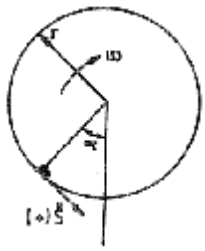

Figure 3.2. The circular motion of a single item

$$\ddot{S} = g \sin\alpha - g \cos\alpha \, \mu_d - \omega^2 r \mu_d \qquad (3.1.)$$

In equation (3.1.) μ_d is the coefficent of friction between the cylindrical surface and granular material.

In order to determine the angle (α_*) at which downward sliding motion starts, it is necessary that the following condition be satisfied:

$$\ddot{S}(\alpha) > \ddot{S}(\alpha_*) = 0 \tag{3.2.}$$

From which,

$$\alpha_* = 2\, tan^{-1}\left(\frac{-1+\sqrt{1+{\mu_d}^2-(w^2 r\mu_d/g)^2}}{\mu_d\,(1-w^2 r/g)}\right) \tag{3.3.}$$

From a review of equation (3.3.) for $\alpha_* > 0$, it follows:

$$\omega < \sqrt{g/r} \tag{3.4.}$$

Relationships (3.2.) - (3.4.) reveal that sliding motion will occur when $\alpha > \alpha_*$.

3.1.2.2. The Motion of Layer of Granular Material along a Circular Path

If the layer of granular material assumed to cover the internal surface of the cylinder is to come to equilibrium at angle of β then from Fig. 3.3 the following can be written:

$$F_{net} = \int_0^{\beta} \ddot{S}\; dm = 0 \tag{3.5.}$$

In equation (3.5.) F_{net} is the net force which moves the layer downwards, $\ddot{S}$ represents the acceleration of the infinitesimal mass with size dm. Besides, designating the bulk density of the granular material by ρ, and the thickness of the layer by e, infinitesimal mass of the layer per unit length (dm) can be expressed as follows:

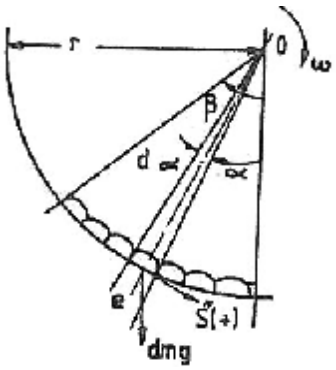

Figure 3.3 Circular motion of the layer of granular material

$$dm = \rho\, r\, e\, d\alpha \qquad \text{or} \qquad m = \rho\, r\, e\, \beta \tag{3.6.}$$

Substituting (3.6.) in (3.5.) and carrying out integration, one obtains the following equation:

$$g\,(1 - cos\beta) - \mu_d\, g\, sin\beta - \mu_d\, w^2\, r\, \beta = 0 \tag{3.7.}$$

Equation (3.7.) is a nonlinear algebraic equation in the unknown β which requires numerical solution. Nevertheless for small β angles an initial solution to start a numerical iteration procedure can be found as follows.

$$sin\,\beta \approx \beta \quad \text{or} \quad cos\,\beta \approx 1 - \beta^2 / 2 \tag{3.8.}$$

$$\beta^2/2 - \mu_d\,(1 + w^2\, r/g)\beta = 0 \tag{3.9.}$$

$$\text{Or} \qquad \beta_1 = 0 \;, \qquad \beta_2 = 2\mu_d\,(1 + w^2\, r/g\,) \tag{3.10.}$$

If relationship (3.4.) is taken into account, the following results:

$$\beta < 4\,\mu_d \tag{3.11.}$$

In order to determine the location (θ_*) of the center of gravity of the layer, the following can be written:

$$\int_0^{\beta} r\, sin\theta\, dm\, g = r\, sin\theta_* m\, g \tag{3.12.}$$

From equation (3.12.) the following is deduced:

$$sin\theta_* = (1 - cos\beta)/\beta \tag{3.13.}$$

Using (13), moment about the cylinder axis (T_o) per unit length of the covered material can be computed by the following equation.

$$T_o = \rho\, r^2\, e\, (1 - cos\beta) g \tag{3.14.}$$

Resultantly, the power (G) required to move the layer along the circular path is estimated by the following:

$$G = T_o\, \omega \tag{3.15.}$$

Energy use due to a single layer transported material in the time interval [t_0, t_n] is evaluated by the following:

$$E = \int_{t_0}^{t_n} G\, dt \tag{3.16.}$$

3.1.2.3. The Motion of a Single Item of Granular Material Along a Helical Path

Referring to Fig. 3.4, the helix angle between the cylinder axis and the helical path, and its complementary angle are designated by ψ , ψ' respectively. Considering that single item of granular material follows the line joining the helicoid and the internal cylindrical surface, the motion of the single item will be resisted by friction forces on these surfaces. Assuming that the coefficient of friction between the item and the cylinder surface is represented by μ_d and that between item and helicoid is μ_h , then the downward acceleration ($\ddot{S}$) of the sliding item turns out to be the following:

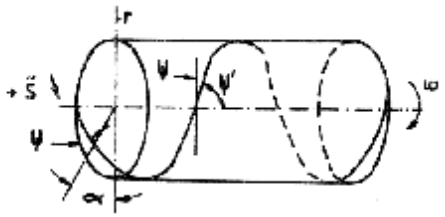

Figure 3.4.Helical motion of a single item

$$\ddot{S}(\alpha) = g \sin\alpha\, (cos\psi - \mu_h sin\psi) - g \cos\alpha\, \mu_d - \omega^2 r \mu_d \tag{3.17.}$$

In accordance with condition (3.2.), the angle (α_*) at which the single item starts sliding along the helical path is found by the following equation:

$$\alpha_* = 2\, tan^{-1}\left(\frac{-A + \sqrt{A^2 + B^2 - C^2}}{B - C}\right) \tag{3.18.}$$

where

$$A = g\,(cos\,\psi - \mu_h\,sin\,\psi)\,, \qquad B = \mu_d\,g\,, \qquad C = w^2\,r\,\mu_d \quad (3.19.)$$

The conditions of sliding motion of the single item along the helical path can be determined by examining equation (3.18.): These conditions are firstly, the limitation of the angular speed of the cylinder as implied by condition (3.4.), which shows the angular speed preventing the sticking of material onto the inner surface at the top. Secondly, the relationship between the helical angle and the coefficient of friction can be deduced as follows:

$$tan\,\psi < 1/\mu_h \quad \text{or} \quad \tan\,\psi' > \mu_h \qquad (3.20.)$$

3.1.2.4. The Motion of Layer of Granular Material along a Helical Path

The fundamental purpose of investigating the bulk motion of the granular material is to determine the amount of granular material to be transported along the cylindrical axis per unit length of the cylinder. It has been shown that a certain relationship can be observed between the circular and the helical motions of the single item. Based on this observation, a similar relationship is expected between the circular and helical motion of bulk material. Comparing circular and helical motions of the single item, conclusions as to how layer of granular material moves along helical path can be drawn.

Based on this comparison, it can be said that the sliding acceleration along the helical path at the same position (α) will be seen to be smaller than that in the case of circular path. In other words, the angle at which sliding will occur for the helical path will be seen to be larger relative to the circular case, due to the fact that:

$$cos\,\psi - \mu_h\,sin\,\psi < 1 \qquad (3.21.)$$

Accordingly, the area of inner cylinder surface covered by the granular material will be larger in the case of helical path as is easily understood from the larger β angle. This is to mean that the mass flow rate of the transported granular material corresponding to helical path will be larger than that of circular path.

Nevertheless, if the assumption that granular material is supposed to continuously cover the inner surface of the cylinder in the form of a single layer is reviewed, it will be realistic to think that some probable gaps will be formed during the motion along the helical path, leading to a more realistic estimation of the mass flow rate by means of circular path case.

To support the discussion above, it is sufficient to note that the angle (β) which results from equation (3.5.) for the case of helical path becomes the following:

$$g\,(1-\cos\beta)(\cos\psi-\mu_h\sin\psi)-\mu_d\,(g\sin\beta+\omega^2 r\,\beta)=0 \qquad (3.22.)$$

Although there is no precise analytical solution of equation (3.22.), for small angles (β) the root of (3.22.) with technical meaning is the following:

$$\beta=\frac{2\,\mu_d}{\cos\psi-\mu_h\sin\psi}\left(1+\frac{w^2 r}{g}\right) \qquad (3.23.)$$

Now, designating transport velocity of the granular material along the cylinder axis by V_z, relative velocity along the helical path by V_s and the tangential cylinder velocity by V_θ the following vector equation can be written:

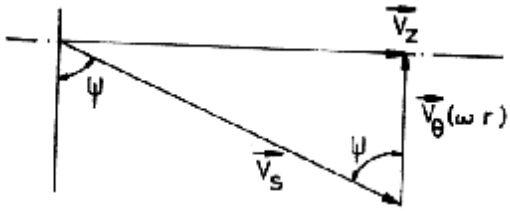

Figure 3.5. Velocity components

$$\boldsymbol{V_z=V_s+V_\theta} \qquad (3.24.)$$

Referring to Fig. 3.5 and to the geometry of the cylinder (Fig. 3.4) the following scalar relationships result:

$$V_\theta=w\,r \qquad (3.25.)$$

$$V_s=w\,r/\cos\psi \qquad (3.26.)$$

$$V_z=w\,r\tan\psi \qquad (3.27.)$$

Consequently, mass flow rate per unit length along the cylinder axis is expressed by the following equation:

$$dm/dt = \rho\, e\, r\, \beta\, V_z \quad (3.28.)$$

3.1.2.5. Granular Material Motion for Combined Circular - Helical Paths

The case considered here is the one whereby layer supposed to move along circular path is forced to move along a helical path. This case concerns the motion in the area between two helicoids attached to the inner surfaces of the cylinder. The sliding conditions are between the two limiting conditions of the circular and helical cases established previously. If the symbols α_{*c}, α_{*h} represent the angles at which sliding occurs along circular and helical paths, respectively, sliding angle α_* corresponding to combined circular – helical path and the relevant acceleration $\ddot{S}(\alpha)$ are bounded by the following relationships.

$$\alpha_{*c} < \alpha_* < \alpha_{*h} \quad (3.29.)$$

$$\ddot{S}_h(\alpha_*) < \ddot{S}(\alpha_*) < \ddot{S}_c(\alpha_*) \quad (3.30.)$$

where $\ddot{S}_h$, $\ddot{S}_c$ designate the accelerations along helical and circular paths, respectively.

Under the case considered the angle (β) at which the layer of granular material comes to equilibrium inside the rotating cylinder, will be affected. If β_c , β_h , β represent the equilibrium angles for motion along circular, helical and combined paths respectively, the following inequality can be written:

$$\beta_c < \beta < \beta_h \quad (3.31.)$$

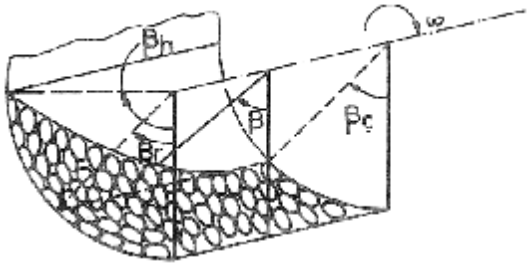

Figure 3.6. Geometry of the layer between two helices

What inequality (31) implies is depicted in Fig. 3.6.

3.1.3. Conditions of Screening

The basic principle underlying size sorting is that an item of a particular size falls into the relevant section by passing through the holes of the screen. Nevertheless, in order for the principle to be materialized, the control over item velocity is essential.

For the purpose of mathematically deriving the expressions related with the velocity control, an item is shown in Fig.3.7 at an initial position before entering the hole of the screen.

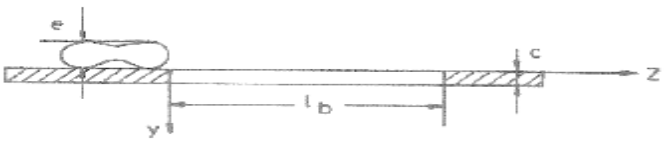

Figure 3.7. Motion of a single item by the sieve hole

If Newton's Second Law is written for the motion of the item in the z and y axes, Fig. 6, the following equations result:

$$d^2z/dt^2 = 0 \quad , \quad d^2y/dt^2 = g \tag{3.32.}$$

Assuming that the item has velocity V_z and zero displacement initially, the solutions of equation set (3.32.) will be following:

$$z = V_z\, t \quad , \quad y = \frac{1}{2} g\, t^2 \tag{3.33.}$$

or

$$y = g\, z^2/(2\, V_z^2) \tag{3.34.}$$

Now, the condition for the item to pass through the hole without hitting its lower corner can be established as such:

$$y \geq c + e \quad , \quad z = l_b \tag{3.35.}$$

where, c, e, l_b are the sheet metal thickness, item thickness, hole length, respectively. If conditions (3.35.) are evaluated in equation (3.34.), the following result is obtained:

$$V_z \leq l_b \sqrt{\frac{g}{2\ (c+e)}} \tag{3.36.}$$

It means that the item velocity in the z direction should be governed by the relation (3.36.).

Similarly, the tangential velocity (V_θ) in the direction perpendicular to cylinder axis should be limited through the following relationship:

$$V_\theta \leq l_a \sqrt{\frac{g}{2\ (c+e)}} \tag{3.37.}$$

where l_a , V_θ are the width of hole and tangential velocity, respectively.

Relationships (3.36.) - (3.37.) imply that the item should have limited velocities along the cylinder axis as well as perpendicular to it for effective screening.

3.1.4. Machine Design

3.1.4.1. Design Principles

In the formation of a design procedure for the cylindrical helical sieve which is to be used for size sorting, the mathematical foundation previously established will be taken into account. This mathematical foundation associates the physical properties of the granular material with the design parameters. The design parameters in question are fundamentally shape and dimensions of screen, cylinder radius, angular velocity, axial velocity of the granular material, cylinder length. The basic physical properties of the granular material are namely, the coefficient of friction with the screen material and the helicoid surface, density, length and thickness of the grain. Besides, the other auxiliary quantity which goes into the design procedure is

the angle of equilibrium (β), which is commonly determined by the granular material properties and the machine characteristics.

Another factor to be taken into consideration in the design is the dimensions of the helicoid surface to be placed inside the cylindrical surface. For all practical purposes, in terms of the diameter (D_d), pitch (h), width (a), the internal (D_i'), and external (D_d') diameters of the ring which will form the helicoid are calculated as follows:

$$D_d' = \sqrt{D_d^2 + \left(h/\pi\right)^2} \quad , \qquad D_i' = D_d - 2\,a \tag{3.38.}$$

3.1.4.2. Design Technique

The mathematical model developed previously will be transformed into a number of ordered steps to form an algorithm yielding the values of the design parameters. In this way, a design technique readily applicable to a computer has come out. Below are given the ordered steps:

i. Desirable mass flowrate and the physical properties of the granular material are entered.
ii. The width and the length of the oblong hole of the sheet metal are selected according to the classification table of granular material. For instance, the references (Guzel et al., 2005; Guzel et al., 2007; Akcali & Guven, 1990; Akcali et al., 2006) are to be referred to when the granular material is peanut.
iii. Helix angle is selected so as to satisfy inequality (3.20.).
iv. Taking into account the sheet metal size corresponding to cylinder radius and length are chosen; and thickness of sheet metal is entered.
v. An angular speed satisfying relation (3.4.) is assumed.
vi. Angle of equilibrium is found by an iteration technique using equation (3.7.) and initial solution (3.10.).
vii. Axial velocity of the granular material is computed by equation (3.27.).

viii. Mass flowrate is calculated by means of equation (3.28.) and the relevant data.

Until the desirable mass flowrate is satisfied the following steps are iterated:

a. Steps starting from number v are repeated.
b. If the steps in the previous iteration (a) do not satisfy the basic mass flowrate criterion, steps starting from number iv are repeated.
c. In case the mass flowrate criterion is not satisfied in the previous step (b), then iteration is started from number iii thereafter.
d. If the basic mass flowrate criterion is still not satisfied in the previous step (c) then iteration is executed from step number ii.

ix. After having approximately obtained equality between desirable and actually calculated values of mass flowrate, the axial velocity is checked with respect to screening condition (3.36.). If the condition (3.36.) has not been realized, the new length of the hole is selected in step number ii and the following steps are iterated until the condition is satisfied.

x. Tangential velocity of the granular material is computed by equation (3.25.) and all the steps starting from number iv are executed until condition (3.37.) is satisfied.

3.1.5. Multi - Layer Theory

Observations in the operation of the machine show that single layer of granular material cannot be maintained throughout the motion of the granular material on the internal surface of the cylinder. Since the efficiency is lower than one hundred percent, this situation is attributed to the formation of layers, one grain on top of the other, a condition underlying the observed loss in the efficiency by preventing the contacting of the above grain from the surface of the cylinder. Thus in order to model the operation of the system realistically there is a need to develop multi layer theory.

The methodology followed for single layer theory will be utilized taking into consideration the varying thickness of the layer.

3.1.5.1. The Motion of Multi- Layer Granular Material along a Circular Path

Single item of the granular material contacting on the surface of the cylinder will have the same acceleration S̈, as given in equation (3.1.)

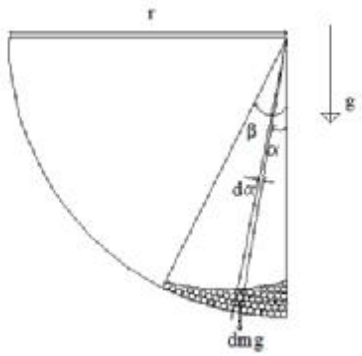

Figure 3.8 Multilayer granular material in cylinder

$$\ddot{S} = g\sin\alpha - g\cos\alpha\,\mu_d - \omega^2 r\mu_d \qquad (3.1.)$$

The layer is modeled as a linearly varying thickness, largest at the lowest point of the cylinder and smallest at the other end, as shown in Figure 3.8.

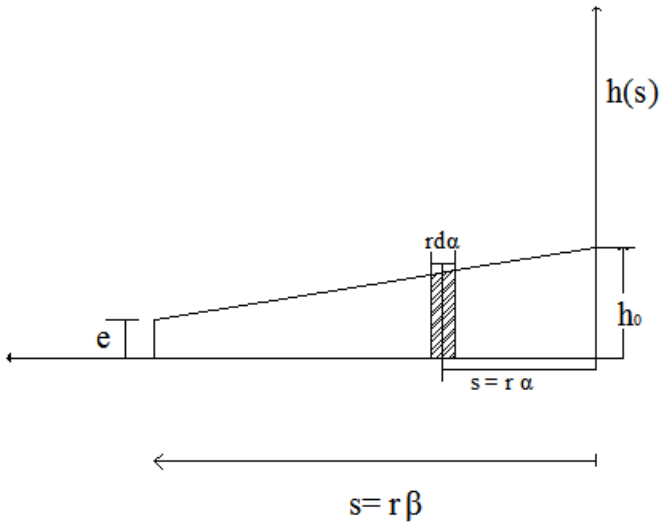

Figure 3.9 Layer thickness variation in terms of developed arc

Referring to Fig.3.9 if the thickness is h_0 when the angular position α is zero and e at the other hand when α is β, then by designating the developed distance from the lowest point of the cylinder upward by s, then the following boundary conditions can be written for layer thickness h in terms of s:

$$h(s) = h_0 \quad \text{at} \quad s = 0 \,, (\alpha = 0) \tag{3.39.}$$

$$h(s) = e \quad \text{at} \quad s = \beta r \,, (\alpha = \beta) \tag{3.40.}$$

Assuming a linear equation as such:

$$h = a + bs \tag{3.41.}$$

The coefficient a and b can be determined by using boundary conditions (3.39.) and (3.40.). The following results are obtained:

$$a = h_0 \tag{3.42.}$$

$$b = \frac{h_0 - e}{r\beta} \tag{3.43.}$$

$$h(s) = h_0 - \frac{h_0 - e}{r\beta} s \tag{3.44.}$$

By using the relationship between developed distance (s) and angular position (α) i.e. $s = r\alpha$, the following forms of layer thickness h can be given:

$$h(\alpha) = e[n - (n-1)\frac{\alpha}{\beta}] \tag{3.45.}$$

$$h(s) = e[n - \frac{(n-1)}{r\ \beta}\ s\ ] \tag{3.46.}$$

$$n = \frac{h_0}{e} \tag{3.47.}$$

where n is the number of layers of the granular material. Infinitesimal mass of the layer per unit length of the cylinder at angular position (α) is formulated as such:

$$dm = \rho\ h\ r\ d\alpha$$

(3.48.)

If equation (3.45.) is used in equation (3.48.) and integrated between 0 and equilibrium angle β, the following result is obtained:

$$m = \left(\frac{h_0+e}{2}\right) \rho r \beta = e \frac{(n+1)}{2} \rho r \beta \quad (3.49.)$$

If equilibrium condition (3.5.) is used together with infinitesimal mass expression (3.48.) and integration is carried out between 0 and angle β the following equation results:

$$F_{net} = \frac{1}{2}\rho r\left[\left(\frac{h_0-e}{\beta}\right)(-2 g \mu_d + r w^2\beta^2\mu_d + 2 g (\beta + \mu_d)\cos\beta + 2 g (\beta \mu_d - 1)\sin\beta - 2 (r w^2 \beta \mu_d - g + g\cos\beta + (g \mu_d h_0 \sin\beta)\right] \quad (3.50.)$$

In order to find equilibrium angle β, when $F_{net} = 0$, the following function can be formed:

$$F(\beta) = g[(\beta(n-\cos\beta) - (n-1)\sin\beta)] - g \mu_d\left[\left(\beta \sin\beta + (n-1)(1-\cos\beta)\right)\right] - \frac{1}{2}\mu_d r w^2\beta^2(1+n) = 0 \quad (3.51.)$$

Since equation (3.51.) is a nonlinear function in the unknown β, a numerical procedure is necessary to find the root of the equation $F(\beta) = 0$. Nevertheless, for small angle β an approximate initial solution is provided by the following relationship:

$$\beta = 2\mu_d\left[1 + \frac{1}{2}(1+n)\frac{r w^2}{g}\right] \quad (3.52.)$$

In order to determine the location (θ_*) of the center of gravity of the layer, the following can be written:

$$\int_0^\beta r \sin\alpha \, dm \, g = r \sin\theta_* m \, g \quad (3.53.)$$

Moment about the cylinder axis (T_o) per unit length of the covered material can be computed by the following equation:

$$T_0 = \int_0^\beta r \sin\alpha \, dm \, g \quad (3.54.)$$

If integration in equation is carried out, upon substitution of (3.48.) in (3.54.) one obtains torque formula as such:

$$T_0 = g e \rho r^2 \left[(n(1-\cos\beta) + (n-1)r\cos\beta) - (n-1)\frac{r}{\beta}\sin\beta\right] \quad (3.55.)$$

Resultantly, the power (G) required to move multilayer of granular material is estimated by the following relationship:

$$G = T_o\ \omega \tag{3.56.}$$

Energy consumed (E) in the time interval [t_n , t_0] is evaluated by the following equation:

$$E = \int_{t_0}^{t_n} G\ dt \tag{3.57.}$$

3.1.5.2. The Motion of Multi-Layer Granular Material along a Helical Path

Using acceleration expression (3.17.) in equilibrium equation (3.5.) together with infinitesimal mass per unit length (3.48.) and also equation (3.45.), and carring out integration between 0 and angle β the following expression is obtained:

$$\mathrm{F_{net}} = \frac{\rho\ r\ e}{\beta}\ \Big[\big(1 + n(\beta - 1)\big)\Big(g\ (cos\psi - \mu_h sin\psi)(sin\beta - \beta cos\beta) + \Big(g - \frac{1}{2} r\ w^2\beta^2 - \ g cos\beta - g\ \beta sin\beta\Big)\mu_d\Big] = 0 \tag{3.58.}$$

There is no analytical solution of equation (3.58.), however for small angles (β) the root of (3.58.) with technical meaning is the following:

$$\beta = \frac{\mu_d(n+1)}{(cos\psi - \mu_h sin\psi)}\ (1 + \frac{w^{\,2} r}{g}) \tag{3.59.}$$

Mass flow rate per unit length along the cylinder axis is expressed by the following equation:

$$\frac{\mathrm{dm}}{\mathrm{dt}} = \int_0^{\beta}\ \rho\ \mathrm{r}\ \mathrm{d}\alpha\ \mathrm{h}\ \mathrm{V_z} \tag{3.60.}$$

If the integration is carried out, the following is obtained:

$$\frac{\mathrm{dm}}{\mathrm{dt}} = \mathrm{e}\frac{(\mathrm{n}+1)}{2}\ \rho\ \mathrm{r}\ \beta\ \mathrm{V_z} \tag{3.61.}$$

3.1.5.3. Solution Procedure for Equilibrium Angle

The algorithm for finding the roots of equilibrium equation (3.51.) for the angle β corresponding to number of layers (n) is given as follows:

i. Firstly, number of layer (n) is entered,
ii. Function of angle β (3.51.) is plotted against β between 0° and 90° ,
iii. Intersection of the function intersection with the abscissa between [0-90] is determined.
iv. This procedure is repeated for different n values.

3.2. Formulation of Efficiency

Performance of the circular helical sieve which is supposed to separate the inflowing granular material into groups with small and big size is formulated with reference to Fig.3.10.

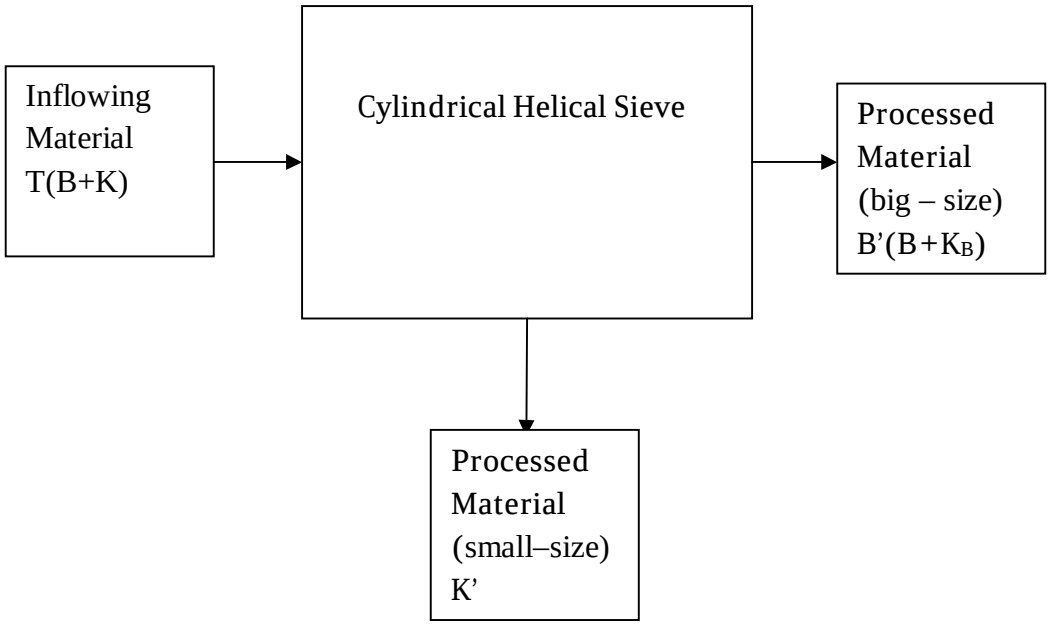

Figure 3.10 Efficiency of the separation process

Performance of circular sieve is based on the input and output relationships. The input to the circular sieve is characterized by total mass T the composition of which consists of small - size group with mass content K and big – size group wit mass content B. From this composition the following ratios can be defined:

$$T=K+B \tag{3.62.}$$

$$r_K = \frac{K}{T} \tag{3.63.}$$

$$r_B = \frac{B}{T} \tag{3.64.}$$

The output from the helical sieve is categorized into two forms of mass represented by small - box contents and large - box contents. The small box contains only items of small size which is designated by mass content K'. The large box has both small – size items with mass content K_B and large – size items with mass content B. Of course, it is assumed that there is no harm to the flowing material during the separation process and that there is no loss of material. Accordingly the following parameters are defined to characterize the output:

$$r'_K = \frac{K'}{K'} = 1 \tag{3.65.}$$

$$r'_B = \frac{B}{K_B+B} \tag{3.66.}$$

Depending on the previously defined parameters above, small – size efficiency (η_K), large – size efficiency (η_B), and the overall efficiency (η) representing system performance are formulated as follows:

$$\eta_K = \frac{K'}{K} \tag{3.67.}$$

$$\eta_B = \frac{B'}{B} = 1 \tag{3.68.}$$

$$\eta = r_K\, r'_K\, \eta_K + r_B\, r'_b\, \eta_b \tag{3.69.}$$

3.3. Experimental Approach

In this section, experimental approach has been implemented on an experimental set- up to determine mass flowrate , torque on the shaft of the machine due to processing of material with or without brushes, instant power and overall energy use with or without brushes in specified intervals of time and efficiency due to the processing of material. Besides, other quantities which affect the experimental outcome such as densities and relevant coefficients of friction on functional surfaces are also subjected to experimental determination.

The elements required for the implementation of the experimental approach including devices and equipment are described in this section. Furthermore, experiments aimed at determining relevant quantities have also been explained.

3.3.1. Experimental Set - Up

Experimental set-up consists of the cylindrical sieve and the collector boxes.

3.3.1.1. Cylindrical Helical Sieve System

There are two main parts in this system. One is the feeder; the other is the cylindrical helical sieve. A gate mechanism connects the feeder to the sieve. There is a screw system which makes it possible to raise and lower the positions of the feeder gate through the enlargement or reduction of the opening area of the feeder gate facial surface. As the cylinder shaft rotates, contacting pin moves on the wavy surface of shaft to let the gate oscillate, the purpose of which is to secure the continuity of flow of granular material from the opening of the feeder to the sieve. The wavy surface on the face of the shaft is produced by small cylindrical slots the size of which fits to that of contacting pin, equally spaced (i.e. at every 90°- angular position) on the face of the shaft. In this way, the oscillation frequency of the feeder gate becomes 4 times the rotational frequency of the machine shaft. The gate mechanism is, in fact, a cylindrical spatial cam mechanism which consists of a

follower pin attached to the gate and a wavy cylinder shaft brought together by means of a spring.

In order to collect system output, two boxes are needed. One is small - size box into which only small - size material drops, the other is big- size box into which large - size material together with some missing small-size material are directed. These boxes are necessary to realize the separation function of the system as well as to minimize the material loss.

The dimensions and technical data associated with the cylindrical helical sieve are presented in Table 3.1.

Table.3.1 Technical data of cylindrical helical sieve

Cylinder radius (r)	0.318 m
Cylinder length	1 m
Sheet metal thickness (c)	1.5mm
Hole width (l_a)	13 mm
Hole length (l_b)	7 mm
Angular velocity	10 rpm
Helix angle	12°
Electrical motor power	0.36 W

3.3.1.2. Granular Material

The granular material that is used in the experiments is kidney beans. Surface quality, geometrical conformity are the basic reasons for selecting kidney beans. When buying kidney beans from the market, length is used as a characteristic dimension. Kidney bean dimensions are measured on a random basis. All the dimensional measurements are collected in Table 3.2. As can be seen from to Table 3.2, maximum length is 6.4 mm for the small bean and minimum length is 8.26 mm for the big beans. At the end of measurements those beans with size larger than 6.4 mm is accepted as big, otherwise small.

Table 3.2 Lengths of Kidney Beans

Big size (mm)	8.36	8.26	8.41	8.82	8.89	9.54	9.96	9.63	9.58	9.32
Small size (mm)	6.14	5.89	6.40	6.24	5.58	5.64	4.98	5.30	5.39	4.39

3.3.2. Measuring Devices

In this section, several measuring devices used in the experiments are included together with their technical features.

3.3.2.1. Power Analyzer

Power analyzer instrument utilized during the experiment is Hioki Power Quality Analyzer 3197 for measuring, monitoring, recording and analyzing the power quality of AC power systems, Fig. 3.11. Technical data has been given in Table 3.3.

Figure 3.11 Power quality analyzer

Table.3.3 Technical data of power analyzer

HIOKI POWER QUALITY ANALYZER 3197 Technical Details	
Measurement line type	Single-phase 2-wire, single-phase 3-wire, three-phase 3-wire, three-phase 4-wire
Voltage range	600.0 V AC
Current ranges	500.0 ma to 5.000 ka AC (depends on current sensor in use)
Power ranges	300.0 W to 9.00 MW (depends on combination of current range and line type)
Basic accuracy	Voltage: ±0.3 % rdg. ±0.2 % f.s. Current: ±0.3 % rdg. ±0.2 % f.s. + current sensor accuracy Active power: ±0.3 % rdg. ±0.2 % f.s. + current sensor accuracy (at power factor=1)
Measurement items	RMS Voltage and Current (200 ms calculation) Voltage (1/2) RMS: one cycle calculation refreshed every half cycle. Current (1/2) RMS: half-cycle calculation. Frequency Active Power/ Reactive Power/ Apparent Power/ Power Factor/ Displacement Power Factor/ Active or Reactive Energy Consumption Demand (Active or Reactive power) Up to 50th Harmonic Analysis (Time series measurement or recording is not capable) Peak Voltage and Current Total harmonic voltage distortion ratio Voltage Unbalance Factor K Factor (Time series recording is not capable) Total harmonic current distortion ratio (Time series recording is not capable)
Number of Recordable Events	50 event waveforms, 20 event voltage fluctuation graphs, 1 inrush current graph, 1000 event counts
Interface	USB 2.0 (Communication to the PC)
Display	4.7-inch color STN LCD
Power supply	AC ADAPTER 9418-15 (100 - 240V, 50/60Hz), BATTERY PACK 9459, Continuous use 6 hours (LCD Back-light auto-OFF 5min.), 23VA max.
Dimensions, mass	128 mm (5.04 in) W × 246 mm (9.69 in) H × 63 mm (2.48 in) D, 1.2 kg (42.3 oz) (with Battery pack)
Supplied accessories	VOLTAGE CORD L9438-55 ×1 (Black×4), AC ADAPTER 9418-15 ×1, BATTERY PACK 9459 ×1, USB Cable ×1, Input Terminal Labels ×1, Input Cord Labels ×1, CD-R (Applications software) ×1, Strap ×1, Carrying case ×1, Measurement guide ×1, Instruction manual ×1

3.3.2.2. Torque Meter

In order to measure the torque on the cylinder shaft, Checkline DIW-75 digital torque meter has been used in experiments. Basic reasons for selecting this device are its convenience in connection with the shaft, suitable interval of torque measurement, digital display, and transfer of measured torque value to a computer. Technical data of the selected torque meter have been presented in Table 3.4.

Table.3.4 Technical data of torque meter

Torque meter technical data	
Measurement:	0.30-75 Nm (55 lb-ft)
Accuracy	±0.5%, ±1 LSD
Sampling Frequency	100 Hz (100 samples/sec)
Display Update Rate	5 Hz (5 times/sec)
USB Output	180 data/sec
Memory	400 data memory for recall or for SPC download
Drive	3/8"

Figure 3.12 Torque meter

3.3.2.3. Camera

A digital camera has been used in finding the angle of equilibrium and, in observing and recording the flow rate pattern. Technical data associated with digital camera are shown in Table 3.5.

Figure 3.13 Digital camera

Table 3.5 Technical data of digital camera

Panasonic NV- GS 500 Technical Details	
General	
Product Type	Camcorder
Width	9.1 cm
Depth	15.3 cm
Height	7.3 cm
Weight	570 g
Main Features	
Camcorder Sensor Resolution	1.0 Mpix
Media Type	Mini DV
Optical Sensor Type	CCD
Optical Sensor Size	1/4.7"
Digital Zoom	700 x
Max Shutter Speed	1/8000 sec
Min Shutter Speed	1/60 sec
Digital Video Format	MPEG-4
Video Capture	MPEG-4 - 320 x 240 - 6 fps
Lens System	
Type	Zoom lens - 3.3 mm - 39.6 mm - f/1.6-2.8
Focal Length	3.3 mm - 39.6 mm
Focus Adjustment	Automatic, manual
Lens Aperture	F/1.6-2.8
Optical Zoom	12 x
Software	Drivers & Utilities, ArcSoft PhotoMontage, ArcSoft PhotoImpression, ArcSoft Panorama Maker
Power	DevicePower adapter + battery charger - external

3.3.2.4. Weight Scale

Electronic weight scale is used for measurements of weight of kidney beans. Technical data have been given in Table 3.6.

Table 3.6 Technical data of weight scale

Technical Detail	
Capacity	5kg
Screen	Low-Battery / Over-Load
Graduation	1g
Display Modes	g/Oz
Size	23x10mm/0.4
Power	4xAAA battery

Figure 3.14 Weight scale

3.3.2.5. Tachometer

Angular velocity of the cylinder shaft is measured by Digital Tachometer. Relevant technical data have been presented in Table 3.7.

Table3.7. Technical Details of Tachometer

Display	Large 5 digit LCD display
Accuracy	±0.05%±1d
RPM Range :	2 to 99,999
Max RPM Resolution	0.1RPM
Range	0-99,999
Memory	Built-in memory recalls Max/Min/Last

Figure 3.15 Digital tachometer

3.3.2.6. Meter

Meter is used for measuring feeder opening and in the manufacturing of some parts of the system such as shaft - torque meter connection, and speed adjustment operation. Division is 1 mm.

Figure 3.16 Meter

3.3.2.7. Chronometer

Electronic chronometer with digital display is used for measuring time for the flow from the feeder to the cylinder. Resolution and accuracies are both 1 second.

Figure 3.17 Chronometer

3.3.2.8. Erlenmeyer Glass

In order to measure volume of the granular material Erlenmeyer glass is used. Division is 10 ml.

3.3.2.9.Protractor

Protractor is used for measuring angles in the in determining coefficient friction Resolution is 1°.

3.3.2.10. Laptop

Laptop is used in the experiments to collect all the digital data coming from digital camera, digital torque meter, and power analyzer.

Technical data associated with laptop have been shown in Table 3.8.

Table 3.8 Technical detail of laptop

Processor	Intel Core 2 Duo P7350 (2,00 GHz, 1066 MHz, 3 MB)
Graphic	ATI Mobility Radeon HD 4650
Storage	320 gigabyte
Display	15.6”
Operating System	Windows 7

3.4. Experiments

3.4.1. Equilibrium Angle

First, grid systems the lines of which are parallel and perpendicular to the shaft axis are drawn on the internal surface of the sieve. At the same time circular grid line in the middle of the cylinder perpendicular to the shaft axis is also marked on the shaft. By means of a digital camera basically positioned along the main axis of

the sieve shaft, camera shots are taken while the machine is operated. Based on the digital camera recordings belonging to a certain cross section of the cylinder, equilibrium angle is measured.

The experiments are also repeated for different feeder gate opening heights varying from 2.0 cm to 3.5 cm with equal 0.5 cm intervals.

3.4.2. Experiment on Bulk Density

The purpose of this experiment is to provide the value of the bulk density needed in the mathematical model and to find the mass flow rate. The following steps are implemented for that purpose: Firstly, the masses of bulk material of big-size and of small-size are measured by means of weight scale and recorded. The bulk material is placed inside the Erlenmeyer glass with volumetric division. Then they are shaken for some time until they are settled with no excessive space between the beans. Their volumes are read off the glass and recorded. Masses are divided by volume values to calculate bulk density.

Experiments are repeated by taking into account different mixing ratios (the ratio of small size material to total mass). In this way, the densities of the mixture are found against different mixing ratios.

3.4.3. Experiment for Coefficient of Friction

In order to determine friction coefficient required in the calculations, a plate made out of material similar to that of the sieve is prepared in the rectangular form. Kidney bean is placed on this plate. By keeping one end of the plate fixed on the ground, the other end is raised gradually giving angular orientation to the plate. Tilting the plate continues until the beans starts sliding on the surface. Then the inclination angle is measured by means of protractor. Tangent of the angle becomes the coefficient of friction.

3.4.4. Efficiency and Flow Rate Experiments

With the purpose of determining performance parameters of the sieve such as efficiency and flow rate, the following steps are executed. By mixing the kidney beans in various proportions with respect to sizes, a specimen of 10 kg mixture is obtained. The mixture is poured into the container while the feeder gate is closed. As soon as the switch of the machine is turned on, chronometer is operated until the feeder box is emptied and the time elapsed for emptying the feeder box is measured and recorded. After the separation process in the cylinder, the amounts of beans that have fallen into small-size and big-size boxes are measured, analyzed and recorded.

The experiments are repeated for the proportions of the small size in the lot varying between 10 - 90 % with equal intervals of 10 %.

The experiments are also repeated for different feeder gate opening heights varying from 2.0 cm to 3.5 cm with equal 0.5 cm intervals.

3.4.5. Experiment on Torque

Torque measurement is needed not only to determine the torque required to the drive the cylinder determine but also to determine the mechanical power consumed by the different parts of the system including material processed and friction due to brushing operation, on the basis of constant angular velocity of the rotating cylinder.

During all the torque measurement the connection between the driving unit (electrical motor and reducer) and accompanying transmission part (belt-drives) is cut off. Instead cylinder shaft is rotated manually through the torque wrench. An intermediate piece for coupling the shaft of sieve with the probe of the torque meter is designed and manufactured.

The experiments are carried out in such a way that torque measurement is taken under two different conditions whereby processed material are on the system together with the brushes, the other includes only brushes (without material) while the cylinder is rotating.

In measuring the torque values, the circumference of the cylinder is divided into twelve parts with equal spacing. This amounts to torque value corresponding to every 30 - degree rotation of the cylinder. The measurements at each marked point of the cylinder are repeated 4 times.

The experiments are repeated at different opening heights of the feeder gate.

All the results are collected in a computer.

3.4.6. Experiment on Power

To measure total energy consumed by the whole system including electrical and mechanical parts such as electrical motor, reducer, bearings, pulley system, spatial cam mechanism, brushes, experiments are carried out using power analyzer by operating the system with or without any material inside with brushes attached and also unloaded system without brushes.

The experiments are repeated at different opening heights of the feeder gate.

All the results are collected in a computer.

3.4.7. Experiment on Energy

Using power analyzer energy under loaded and unloaded conditions with and without brush are measured and recorded. By taking difference between the energy values when there is load and no load in the system and also when there are brush and no brushes, energy only due to processed material and also energy consumed only by brushes are calculated.

Calculations are repeated for each feeder gate height.

4. RESULTS AND DISCUSSION

In this section, results of bulk density, equilibrium angle, coefficient of friction, efficiency, mass flow rate, torque and energy consumption experiments will be presented in graphical and/or tabular forms.

4.1. Equilibrium Angle

Following the procedure of section 3.1.5.3., exemplary values of the equilibrium angle (β) as calculated according to formula (3.51.), are tabulated in Table 4.1. Its graphical form is displayed in Fig. 4.1.

Table 4.1 Number of layer n=1

Number of layer (n)	Equilibrium Angle (β) (°)	Equilibrium Angle (β) (rad)	Result
1	0	0	0
1	1	0,017453	-0,00098
1	10	0,174533	-0,07401
1	20	0,349066	-0,18775
1	30	0,523599	-0,17726
1	31	0,541052	-0,16317
1	32	0,558505	-0,14607
1	33	0,575959	-0,12582
1	34	0,593412	-0,10226
1	35	0,610865	-0,07525
1	36	0,628319	-0,04464
1	37	0,645772	-0,01028
1	38	0,663225	0,027975
1	39	0,680678	0,070267
1	40	0,698132	0,116737
1	50	0,872665	0,840781
1	60	1,047198	2,121002
1	70	1,22173	4,056361
1	80	1,396263	6,712996
1	90	1,570796	10,11996

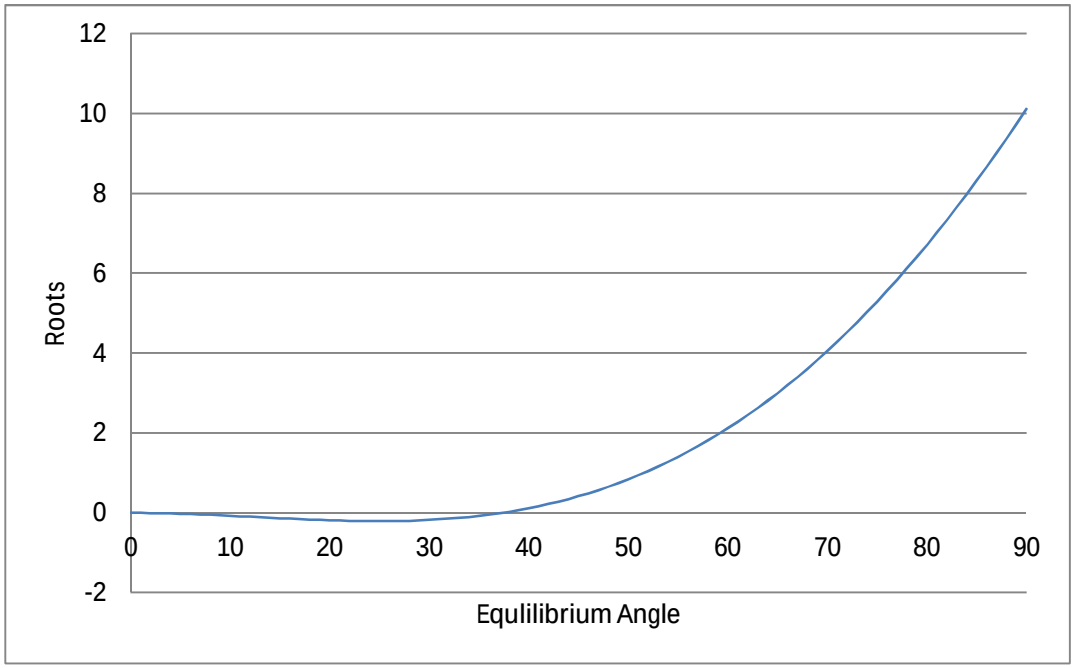

Figure 4.1 Theoretical equilibrium angle

Theoretical equilibrium angles corresponding to different numbers of layers (n) have been collected in Table 4.2. The graphical form of Table 4.2 is shown in Fig.4.2 in which abscissa is number of layer (n) and the ordinate is equilibrium angle (β). By non - linear regression the expression between equilibrium angle and number of layer is found to be:

$$\beta = -0{,}0139n^2 + 0{,}1211n + 0{,}5457 \qquad (4.70.)$$

It is observed that equilibrium angle increases with increasing number of layers. Furthermore, the slope of the curve in Fig.4.2 decreases with increasing number of layers. This point is supported by the derivative expression of equation (4.70.), given as follows:

$$d\beta/dn = -0{,}0278n + 0{,}1211 \qquad (4.71.)$$

If the slope of angle (β) is plotted against number of layers (n), the resulting curve is seen in Fig. 4.3. From Fig. 4.3 it is deduced that slope goes to zero when n is 4,339069. In this case equilibrium angle has an asymptotic value as implied by Fig. 4.3.

Table.4.2 Theoretical equilibrium angle against - number of layer

Number of Layer	1	1,25	1,5	1,75	2	2,25	2,5	2,75	3	3,5
Theoretical Equilibrium Angle	37,28	38,73	39,97	41,05	41,98	42,83	43,56	44,22	44,82	45,86

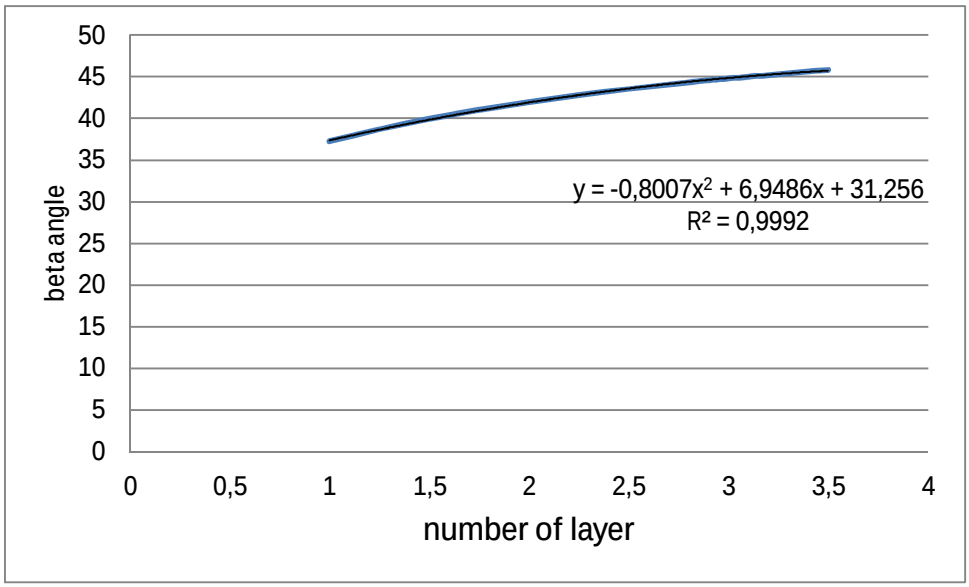

Figure 4.2 Theoretical equilibrium angle vs Number of layer

Table. 4.3. Number of layer- result of equation (4.71.)

root	1	1,25	1,5	1,75	2	2,25	2,5	2,75	3	3,5	4	4,25	4,32	4,33	4,33 9069
result	5,34 72	4,94 685	4,54 65	4,14 615	3,74 58	3,34 545	2,94 51	2,54 475	2,14 44	1,34 37	0,54 3	0,14 265	0,03 0552	0,01 4538	1,49 E-05

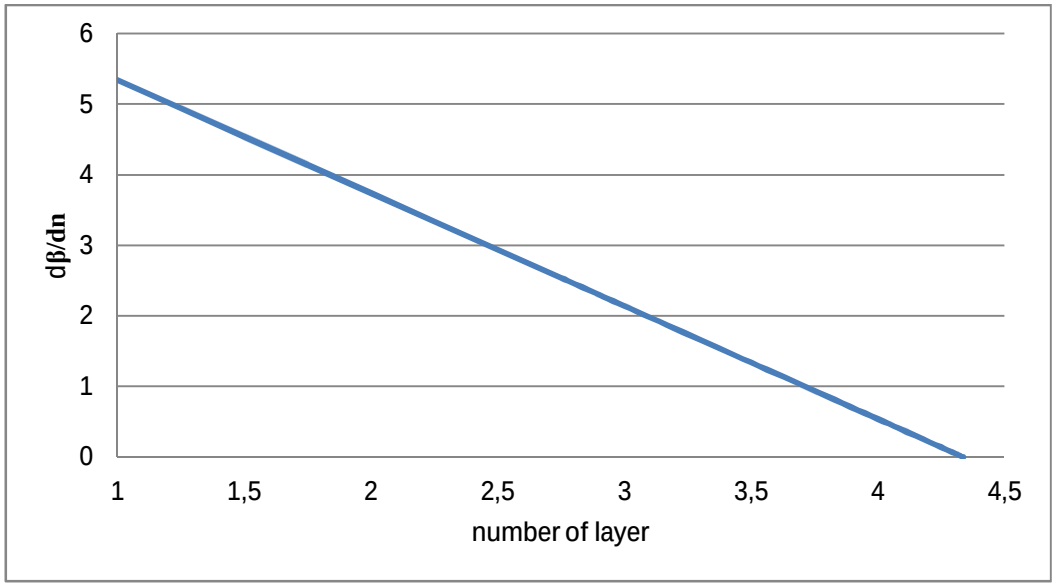

Figure 4.3 dβ/dn vs number of layer

On the other hand, the camera shots taken during the experiments carried out according to section 3.4.1 are displayed in Figures 4.4 - 4.7 corresponding to feeder gate heights of 2cm - 3.5cm with 0.5 cm intervals, respectively. By using image processing software (Corel Draw X5) equilibrium angles are measured from Fig. 4.4 - 4.7. The measurement results are collected in Table 4.4. When the values in Table 4.4 are plotted on a pair of axis the resulting curve turns out to be the one shown in Fig. 4.8. By non- linear regression the equation of the curve is the following:

Figure 4.4 Equilibrium Angle for 2cm feeder gate height

Figure 4.5 Equilibrium angle for 2.5cm feeder gate height

Figure 4.6 Equilibrium angle for 3 cm feeder gate height

Figure 4.7 Equilibrium angle for 3.5 cm feeder gate height

$$\beta = -0{,}0139x^2 + 0{,}1211x + 0{,}5457 \quad (4.72.)$$

where x represents the opening height of the feeder gate in cm.

Table.4.4. Experimental values of equilibrium angles

Feeder Gate Heights (cm)	2.0	2.5	3.0	3.5
Equilibrium Angles (°)	37.58	38.96	40.26	43.19
Equilibrium Angles (rad)	0.655895	0.67998	0.70267	0.753808

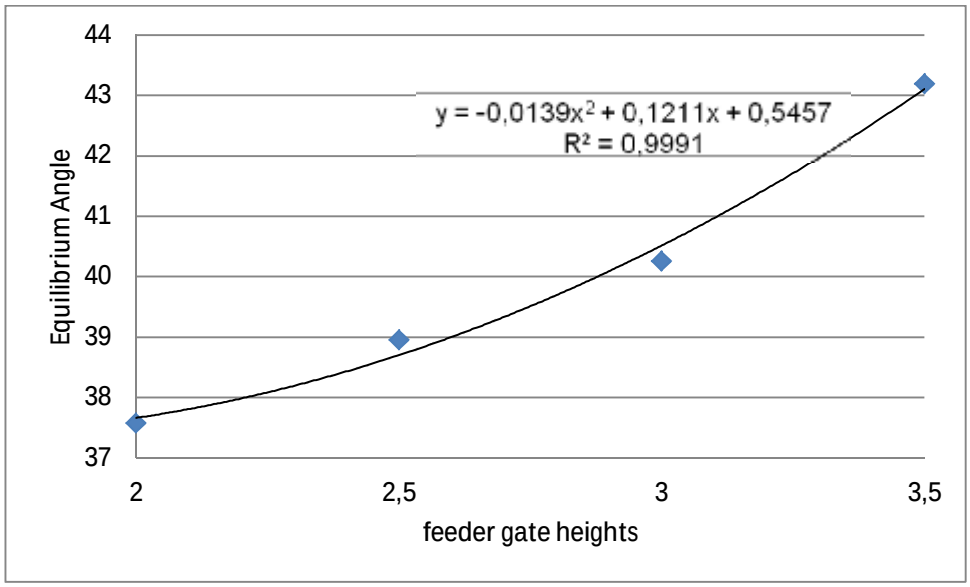

Figure 4.8 Equilibirum angle vs feeder gate heights

By comparison of experimental values with the theoretical values semi-empirical values of number of layers are determined and the results are tabulated in Table 4.5. When the values in Table 4.5 are plotted on a pair of axis the resulting curve turns out to be the one shown in Fig. 4.9. As feeder gate height is increased, number of layer also increases.

Table.4.5 Semi – empirical relationships between equilibrium angle and number of layer and feeder gate height.

Feeder gate heights (cm)	Number of layer	Equilibrium Angle (°)	Equilibrium Angle (rad)
2.0	1.032	37.58	0.65589
2.5	1.304	38.96	0.67998
3.0	1.584	40.26	0.70267
3.5	2.355	43.19	0.75380

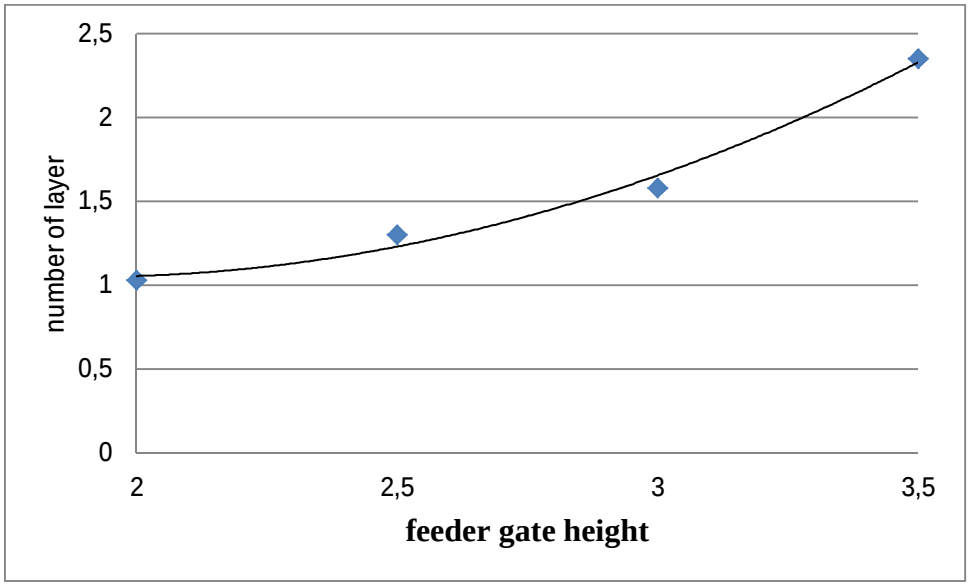

Figure 4.9 Number of layer vs. feeder gate heights

4.2. Bulk Density

Implementing guidelines mentioned in 3.4.2. the following results are obtained and collected in Table 4.6. If the values in Table 4.6 are transformed into graphical form, the straight line shown in Fig.4.10 results. The equation of straight line is found to be as follows:

$$\rho = 0{,}0466\, r_K + 0{,}7344 \qquad (4.73.)$$

Table.4.6 Mixture Bulk Density

Big - Size Kidney Beans Mass (gr)	Small - Size Kidney Beans Mass (gr)	Mixture Volume(ml)	Small - Size Ratio(r_k)	Mixture Bulk Density
0	500	640	1	0,78125
125	375	650	0,75	0,76923
250	250	660	0,5	0,75757
375	125	670	0,25	0,74626
500	0	680	0	0,73529

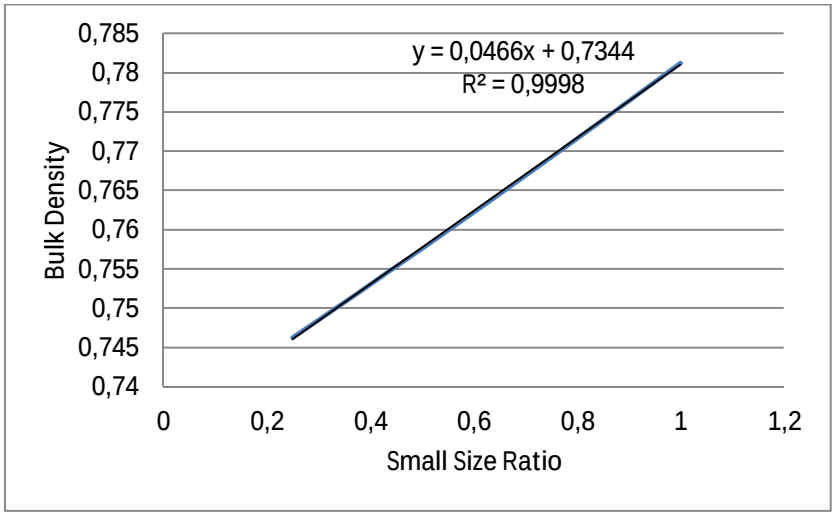

Figure 4.10 Measured bulk density vs small size ratio

4.3. Coefficient of Friction

Coefficient of friction experiments explained in section 3.4.3 have been applied and the resulting values are tabulated in Table 4.7.

Table.4.7 Coefficient of friction values

Experiment Number	1	2	3	Average	Standard Deviation
Results	0,3249	0,3315	0,3176	0,3246	0,005677

4.4. Efficiency and Flow Rate

Efficiency and flow rate experiments described in section 3.4.4 have been carried out to yield results tabulated according to the specific feeder gate heights in Table 4.8 to Table 4.11. Efficiency values contain in Tables 4.8 - Table 4.11have been plotted against small- size ratio as shown in Fig. 4.11.

Table.4.8 Experiment result for 2 cm feeder height

Exp. No.	input		Dropped into box		Time (s)	Mass Flow rate (kg/s)	Efficiency (%)
	Big size Kidney beans (g)	Small size Kidney beans (g)	Big size Kidney beans (g)	Small size Kidney beans (g)			
1	9000	1000	9007	993	87,13	0,114771	99,86005
2	8000	2000	8014	1986	83,6	0,119617	99,72024
3	7000	3000	7018	2985	80,75	0,123839	99,67046
4	6000	4000	6018	3977	74,96	0,133404	99,59054
5	5000	5000	5030	4963	70,08	0,142694	99,33179
6	4000	6000	4049	5951	64,03	0,156177	99,02593
7	3000	7000	3062	6938	59,34	0,16852	98,77255
8	2000	8000	2080	7920	52,96	0,188822	98,43077
9	1000	9000	1070	8930	49,12	0,203583	98,64579

Table.4.9 Experiment result for 2.5 cm feeder height

Exp. No.	input		Dropped into box		Time(s)	Mass Flow rate (kg/s)	Efficiency (%)
	Big Kidney beans (g)	Small Kidney beans (g)	Big Kidney beans (g)	Small Kidney beans (g)			
1	9000	1000	9015	985	42,39	0,235905	99,70025
2	8000	2000	8019	1981	41,8	0,239234	99,62045
3	7000	3000	7035	2965	38,47	0,259943	99,30174
4	6000	4000	6049	3951	36,81	0,271665	99,02397
5	5000	5000	5058	4942	33,81	0,29577	98,84665
6	4000	6000	4097	5903	32,92	0,303767	98,08297
7	3000	7000	3097	6903	32,22	0,310366	98,09038
8	2000	8000	2098	7902	31,12	0,321337	98,08578
9	1000	9000	1094	8906	30,78	0,324886	98,20077

Table.4.10 Experiment result for 3 cm feeder height

Exp. No.	input		Dropped into box		Time(s)	Mass Flow rate (kg/s)	Efficiency (%)
	Big Kidney beans (g)	Small Kidney beans (g)	Big Kidney beans (g)	Small Kidney beans (g)			
1	9000	1000	9031	969	31,21	0,32041	99,38106
2	8000	2000	8079	1921	30,03	0,333	98,42772
3	7000	3000	7085	2915	29,75	0,336134	98,3102
4	6000	4000	6101	3899	28,34	0,352858	97,99672
5	5000	5000	5113	4887	27,91	0,358295	97,76497
6	4000	6000	4146	5854	25,96	0,385208	97,13141
7	3000	7000	3163	6837	23,31	0,429	96,824
8	2000	8000	2175	7825	21,13	0,473261	96,6408
9	1000	9000	1153	8847	20,94	0,477555	97,14303

Table.4.11 Experiment result for 3.5 cm feeder height

Exp. No.	input		Dropped into box		Time(s)	Mass Flow rate (kg/s)	Efficiency (%)
	Big Kidney beans (g)	Small Kidney beans (g)	Big Kidney beans (g)	Small Kidney beans (g)			
1	9000	1000	9098	902	21,89	0,45683	98,05056
2	8000	2000	8115	1885	21,56	0,463822	97,7163
3	7000	3000	7116	2884	20,01	0,49975	97,69891
4	6000	4000	6150	3850	19,11	0,523286	97,03659
5	5000	5000	5173	4827	18,94	0,527983	96,59786
6	4000	6000	4239	5761	18,21	0,549149	95,35475
7	3000	7000	3253	6747	17,79	0,562114	95,13677
8	2000	8000	2257	7743	15,97	0,626174	95,15264
9	1000	9000	1265	8735	15,44	0,647668	95,25514

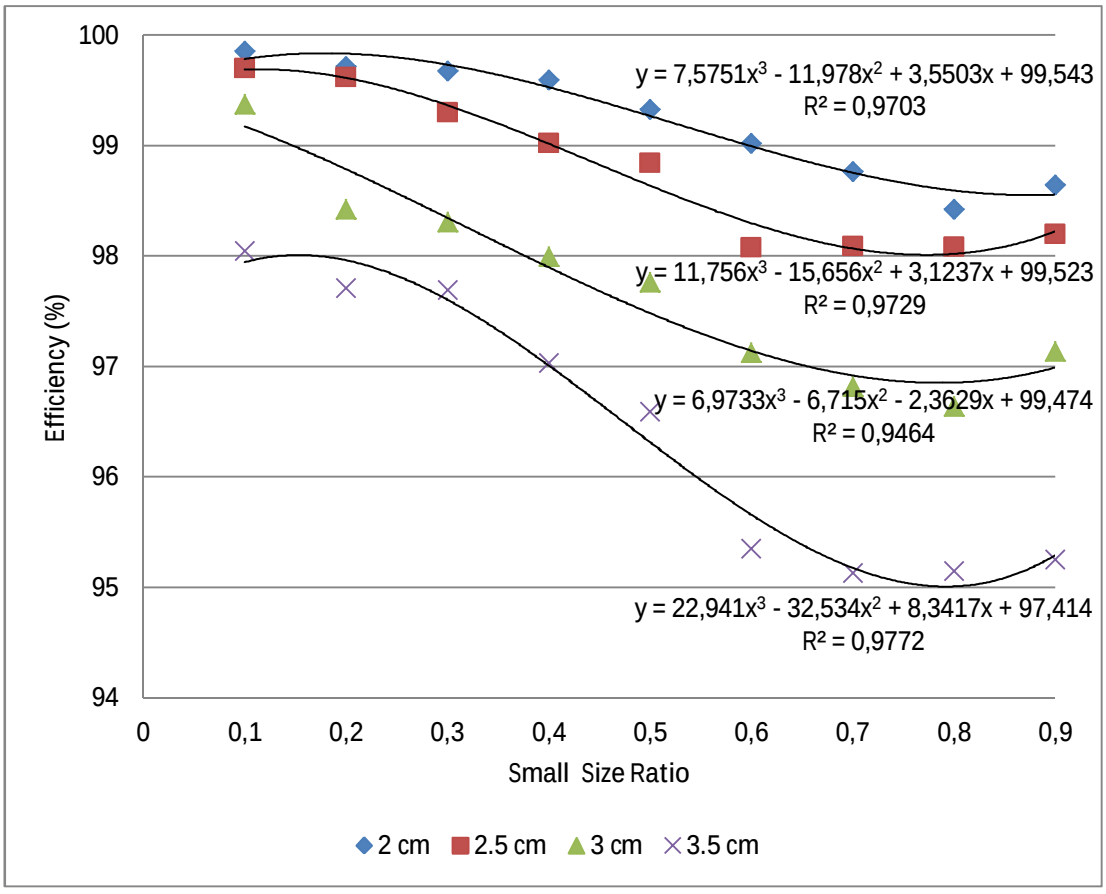

Figure 4.11 Efficiency vs small - size ratio

From Fig. 4.11 efficiency values are observed to decrease against increasing small- size ratio up to a certain point and then have appeared to stabilize. When the feeder gate height is increased efficiencies have decreasing tendencies.

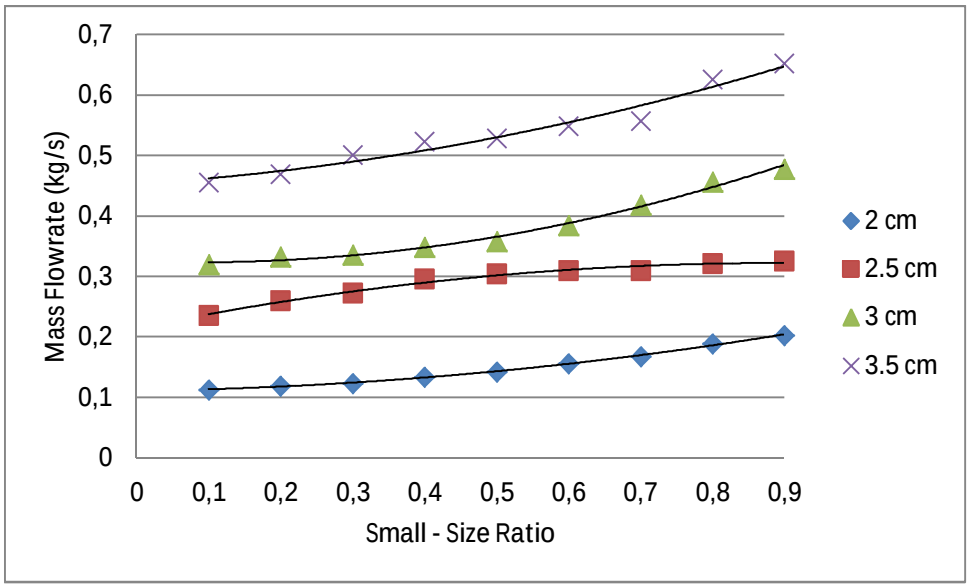

Figure 4.12 Mass flow rate vs small - size ratio

Upon evaluating the mass flow rate values against small- size kidney bean composition the curve shown in Fig. 4.12 results. As the small – size ratio increases, mass flow rate increases. When the opening height of the feeder gate is increased flow rate increases too.

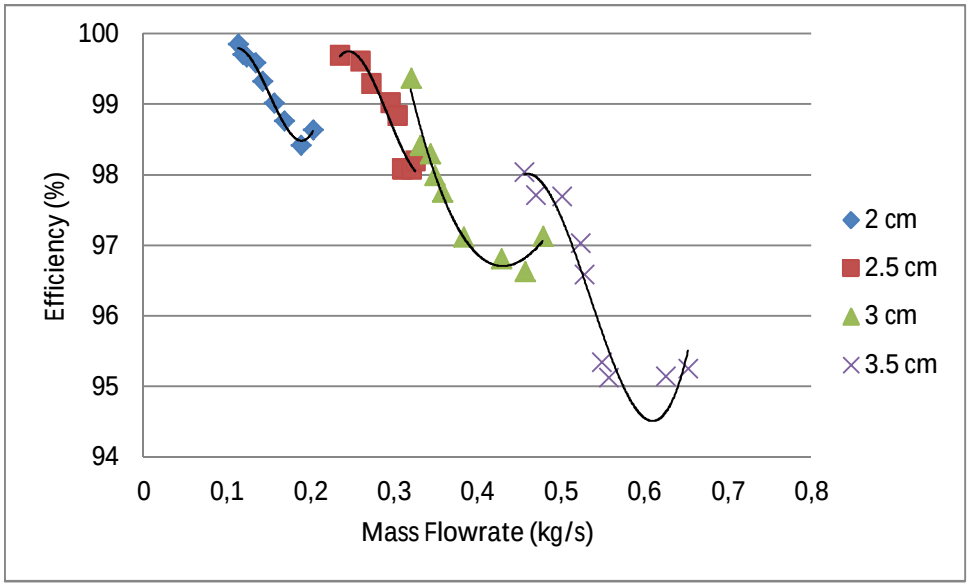

Figure 4.13 Efficiency vs mass flow rate

Based on the efficiency and mass flow rate values from Tables 4.8 to Table 4.11 efficiency vs mass flow rate curve has been drawn in Fig.4.13. Efficiency is seen to be influenced by the mass flow rate negatively meaning that as the gate height is raised mass flow rate becomes larger leading to decreasing efficiencies. Although efficiency shows decreasing tendencies with increasing mass flow rate, after a certain point they appear to be constant. The efficiency never drops below 95 % within the operating conditions.

4.5. Torque

Torque experiment has been explained in section 3.4.5. Torque values collected from the experiments without and with brush are collected in Table 4.12 and Table 4.13, respectively. It is observed that the average torque values corresponding to one revolution of the cylinder without and with brush are 3,058654Nm and 4, 935192Nm respectively. From these values it is observed that brushes require approximately 38 % of the driving torque applied on the machine, when there are no kidney beans in the cylinder.

When the machine is operated with kidney beans with different feeder gate heights, the torque values tabulated in Table 4.14 are obtained. These values include the effects of load, brush and other factors like friction in the transmission elements such as belt – drives, reducer units, bearings etc.

The average torque values in Table 4.14 are plotted against feeder gate heights in Fig.4.14. It is seen that a quadratic function relationship exist between the feds to the behavior torque and gate height. When the feeder gate height is increased, torque values get larger. In order to isolate effects of the load on the machine, the differences between the torque values with load (Table 4.14) and without load (Table 4.13) have been taken into consideration leading to the curve in Figure 4.15. When the feeder gate is positioned at increased heights the flow rate will increase hence will induce larger torques on the system. For instance, when the feeder gate height is increased from 2 cm to 3.5 cm, torque almost doubles.

Table.4.12 Unloaded Torque Values without Brush

Points	Experiment no.				Average	Standard Deviation
	1	2	3	4		
0	2,54	2,03	1,93	2,07	2,1425	0,209713
1	1,96	2,56	2,24	2,36	2,2800	0,216333
2	4,95	5,98	5,23	4,85	5,2525	0,442371
3	5,36	5,65	6,76	6,20	5,9925	0,374306
4	8,42	8,28	8,38	8,21	8,3225	0,077409
5	4,58	3,49	4,29	4,25	4,1525	0,397231
6	1,15	1,76	1,60	1,63	1,535	0,227967
7	1,25	0,91	1,47	1,51	1,285	0,21936
8	1,07	1,11	1,04	1,11	1,0825	0,020425
9	1,21	1,41	1,28	1,42	1,33	0,085
10	1,87	2,13	1,97	2,37	2,085	0,179913
11	1,98	2,20	1,84	2,15	2,0425	0,100335
12	2,01	2,23	2,35	2,45	2,26	0,157718
Average (Nm)						3,058654

Table 4.13 Unloaded Torque Values with Brush

Points	Measurement Number 1	2	3	4	Average	Standard Deviation
0	5,24	5,76	5,48	4,95	5,3575	0,292348
1	1,99	2,32	2,03	1,87	2,0525	0,164901
2	6,36	6,21	6,15	6,38	6,275	0,074958
3	5,91	5,42	5,1	4,61	5,26	0,46653
4	8,63	8,58	9,32	9,48	9,0025	0,369212
5	5,46	5,18	5,26	5,51	5,3525	0,128568
6	9,42	9,8	9,23	9,64	9,5225	0,159153
7	1,49	1,61	1,02	1,07	1,2975	0,21591
8	1,26	1,12	1,27	1,04	1,1725	0,083619
9	4,91	4,76	4,83	4,23	4,6825	0,256183
10	3,46	3,11	3,06	3,36	3,2475	0,138491
11	5,67	5,99	5,5	5,72	5,72	0,137295
12	5,04	5,54	5,14	5,14	5,215	0,188331
Average (Nm)						4, 935192

Table.4.14 Loaded Torque Values With Brush

Points	Feeder Gate Heights 2 cm	2.5 cm	3 cm	3.5 cm
0	7,10	10,46	11,50	13,10
1	11,16	12,35	14,40	15,32
2	9,25	14,80	14,01	15,10
3	13,75	11,85	20,80	19,50
4	12,10	14,60	22,30	18,79
5	15,40	15,43	22,60	23,10
6	15,80	16,80	24,30	30,30
7	8,80	11,50	16,05	27,60
8	6,02	10,05	12,90	20,80
9	5,90	10,30	12,50	16,70
10	8,20	8,26	13,30	15,15
11	8,80	10,5	11,40	16,20
12	8,05	9,90	13,60	17,50
Average (Nm)	10,02	12,06	16,12	19,16

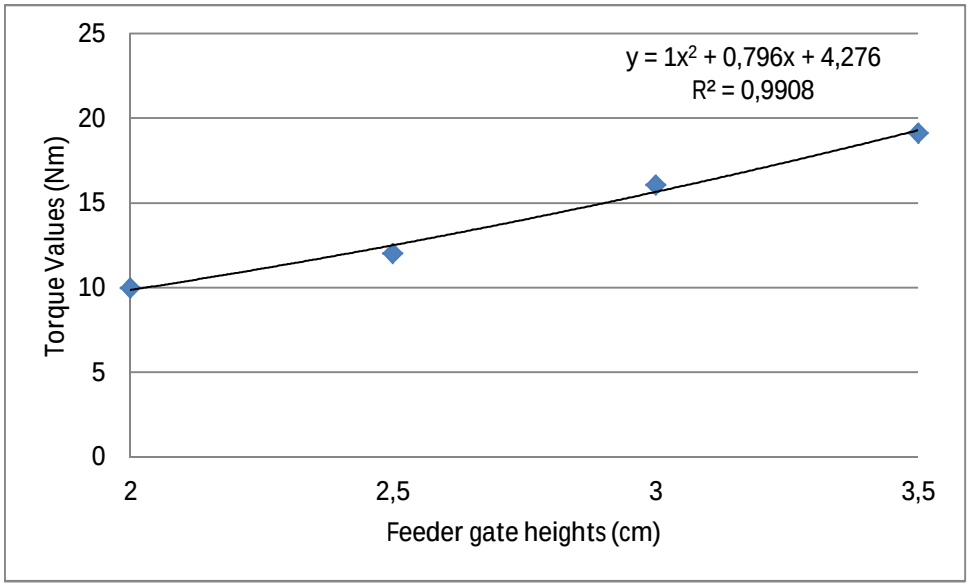

Figure 4.14 Experimental torque values vs feeder gate heights

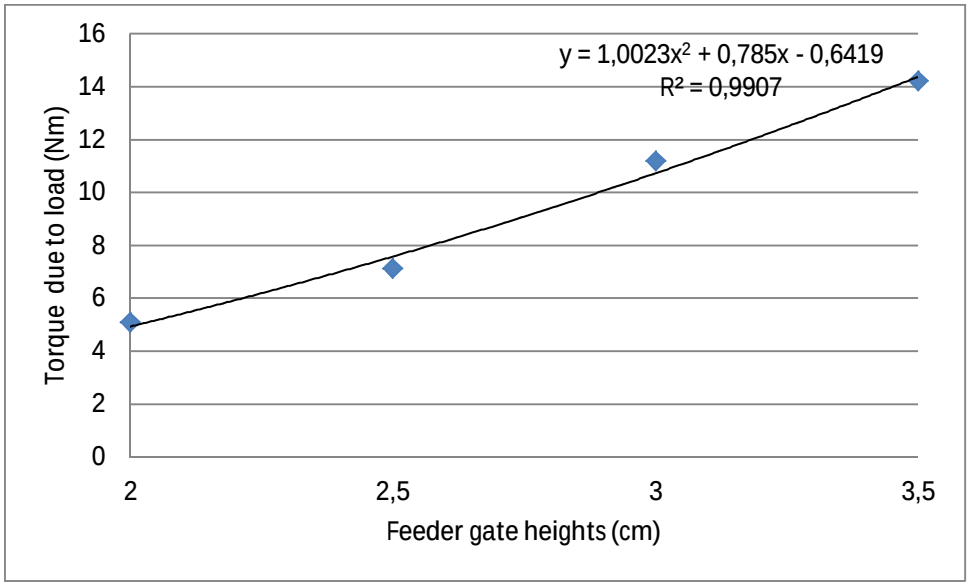

Figure 4.15 Experimental torque due to load vs. feeder gate height

Theoretical torque values have been calculated according to formula (3.55.). By taking into consideration the experimental conditions summarized in Table 4.15, theoretical torque values vs. number of layer are calculated and collected in Table 4.16. Its graphical form is displayed in Fig.4.16. In view of the results summarized in Table 13 the torque values versus feeder gate heights are calculated and tabulated in Table 4.17. As can be seen from Fig. 4.17, as the feeder gate height increases,

torque values also increase. From Fig.4.18 it is clearly observed that theoretical and experimental torque behavior under similar operating conditions agree with each other.

Table 4.15 Values of Parameters in Theoretical Torque Calculation

Bean thickness (e)	Gravitation acceleration (g)	Radius of cylinder (r)	Bulk Density (ρ)	Angular Speed of Cylinder (w)
6 mm	9,80665 m/s^2	0,318 m	744,69 kg/m^3	1,047 rad/s

Table 4.16. Theoretical Torque Values

Number of Layer (n)	Beta Angle (°)	Beta Angle (rad)	Torque (T) (Nm/m)
1	37,28	0,650328889	9,044347
1,25	38,73	0,675623333	11,52778
1,5	39,97	0,697254444	13,88164
1,75	41,05	0,716094444	16,04435
2	41,988	0,732457333	17,95364
2,25	42,83	0,747145556	19,58566
2,5	43,563	0,759932333	20,87996
2,75	44,226	0,771498	21,83051
3	44,824	0,781929778	22,40923
3,25	45,37	0,791454444	9,415314
3,5	45,86	0,800002222	12,01771

Table 4.17 Experimental and Theoretical Torque Values due to Load

Experiment Torque Values (Nm)	Theoretical Torque Value (Nm)	Feeder gate heights(cm)	Number of layer
5,084808	4,480122	2	1,032
7,124808	7,08252	2,5	1,304
11,18481	9,635365	3	1,584
14,22481	15,27262	3,5	2,355

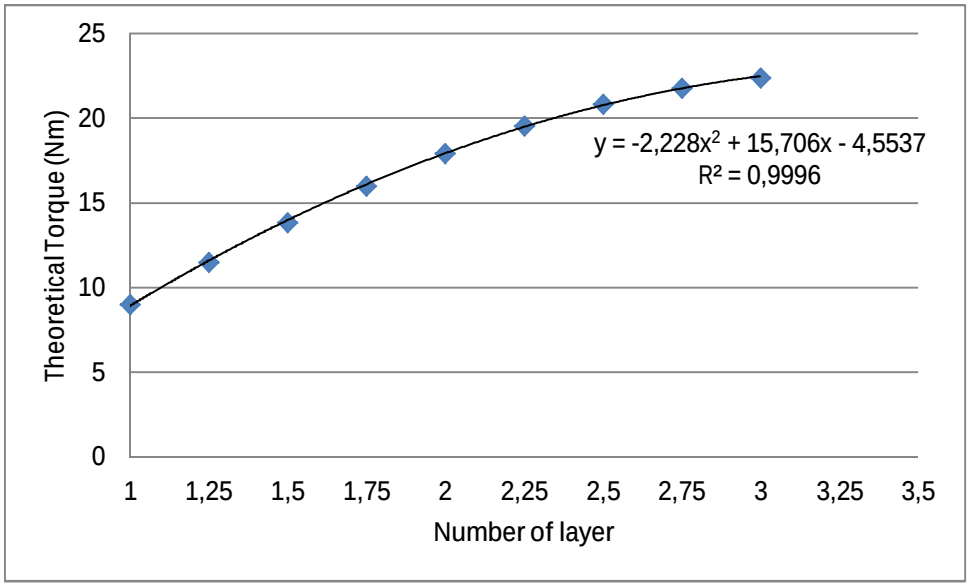

Figure 4.16 Theoretical torque vs. number of layer

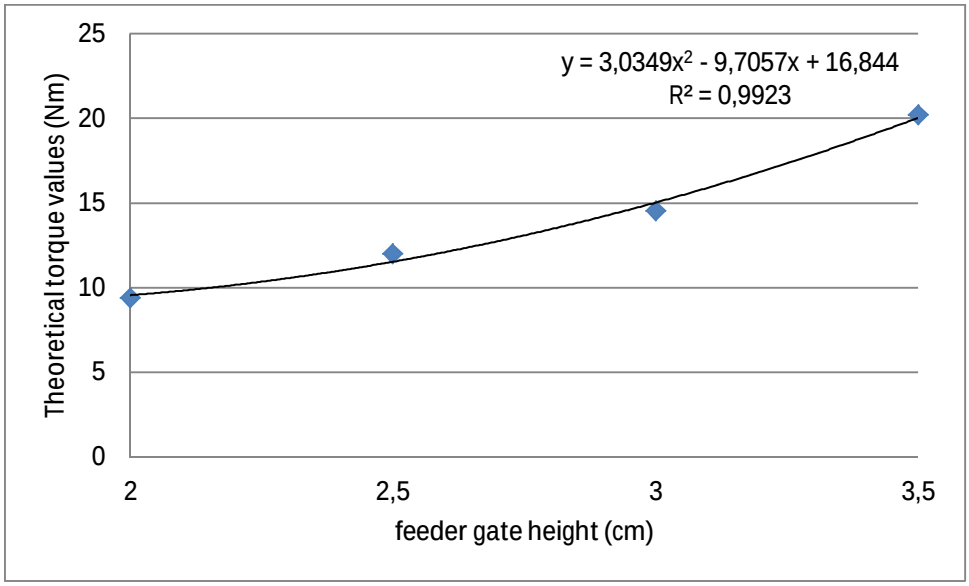

Figure 4.17 Theoretical torque values vs. feeder gate heights

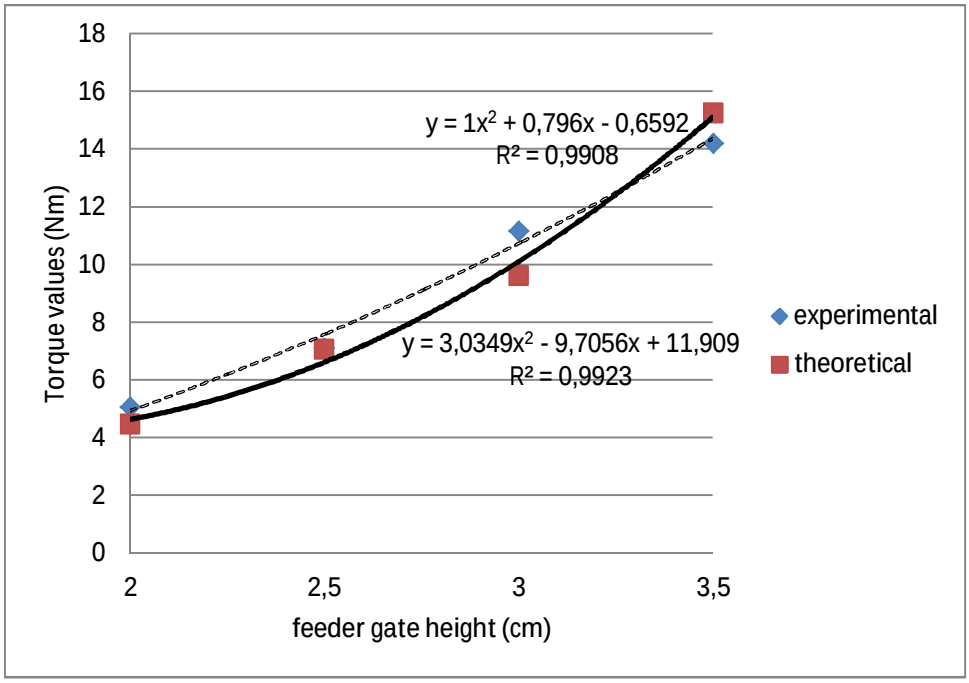

Figure 4.18 Experimental and theoretical torque values due to load vs. feeder gate heights

4.6. Power

Power experiments have been explained in section 3.4.6. Unloaded power measurements over 91- second time span are recorded and displayed in Fig.4.19. When the power values with brush are subtracted from those without brush, power consumption due to only brush effect is deduced as shown in Fig. 4.20. Under unloaded conditions average brush consumption over the given time span turns out to be 9,03 W.

Under normal operating conditions loaded experimental power values are recorded against time and the resulting curves are shown in Fig 4.21. When the differences between the loaded and unloaded power measurements for different gate heights are computed, results exhibited in Table 4.18 are obtained. Experimental power values due to load, corresponding to different feeder gate heights have been plotted in Fig.4.22. From Fig.4.22 average and standard deviation values of experimental power corresponding to different feeder gate heights have been computed and tabulated in Table 4.18. Most of the time standard deviation is less

than 1 %. By plotting average experimental power against feeder gate heights the curve shown in Fig. 4.23 is obtained. It's observed that from Fig.4.23 there is a quadratic relationship between the power values and feeder gate heights.

Theoretical power values have been calculated from equation (3.55.) and (3.56.) under the experimental conditions shown in Table 4.15. Then the resulting theoretical power values versus different feeder gate heights are plotted in Fig.4.24 by making use of Table 4.15. As can be seen in Table 4.19 it is observed that theoretical and experimental power behaviors under similar conditions are in harmony with each other.

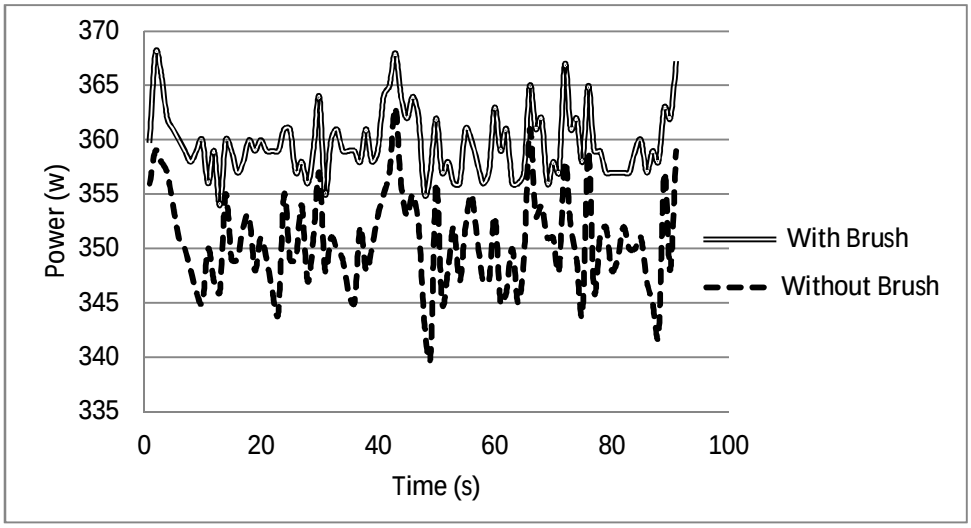

Figure 4.19 Unloaded experimental power with and without brush vs. time

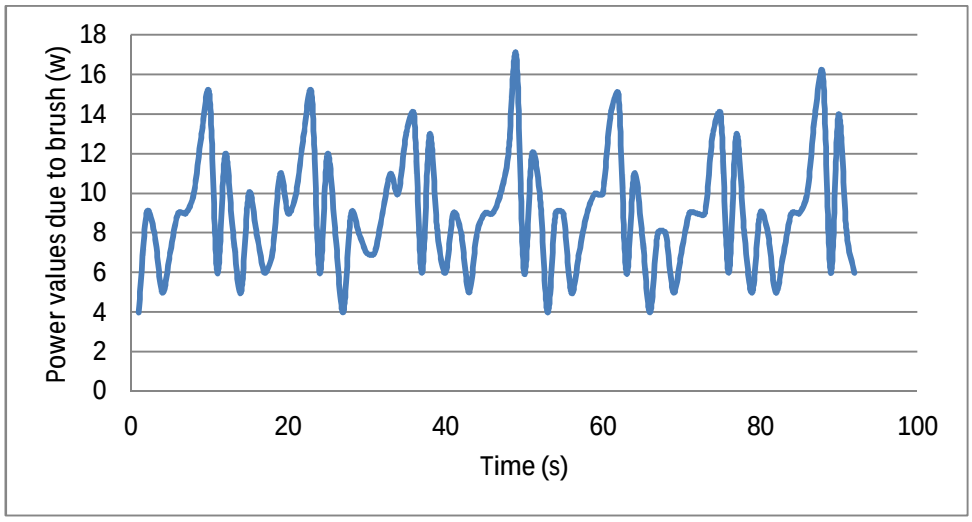

Figure 4.20 Power values due to brush vs time

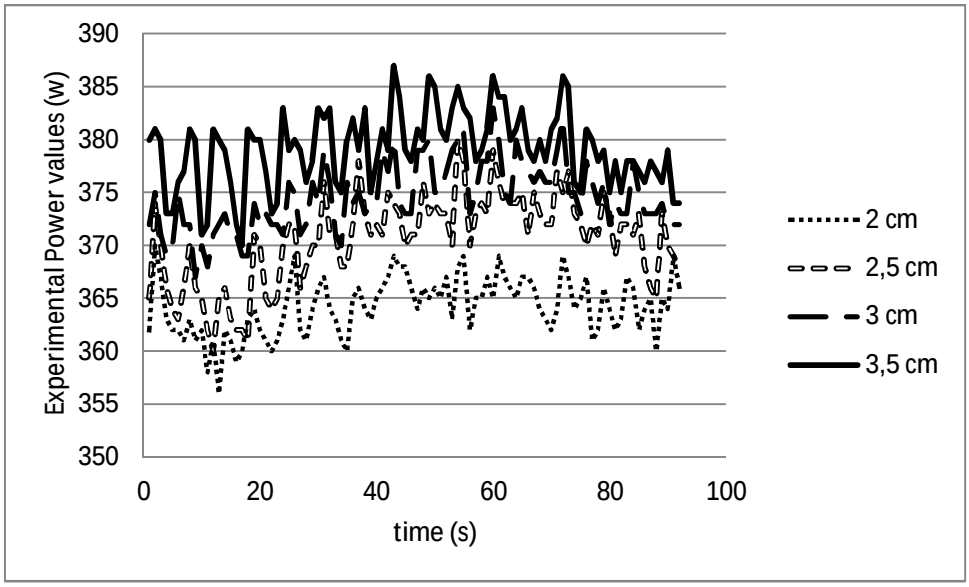

Figure 4.21 Loaded experimental power vs. time for different feeder gate heights

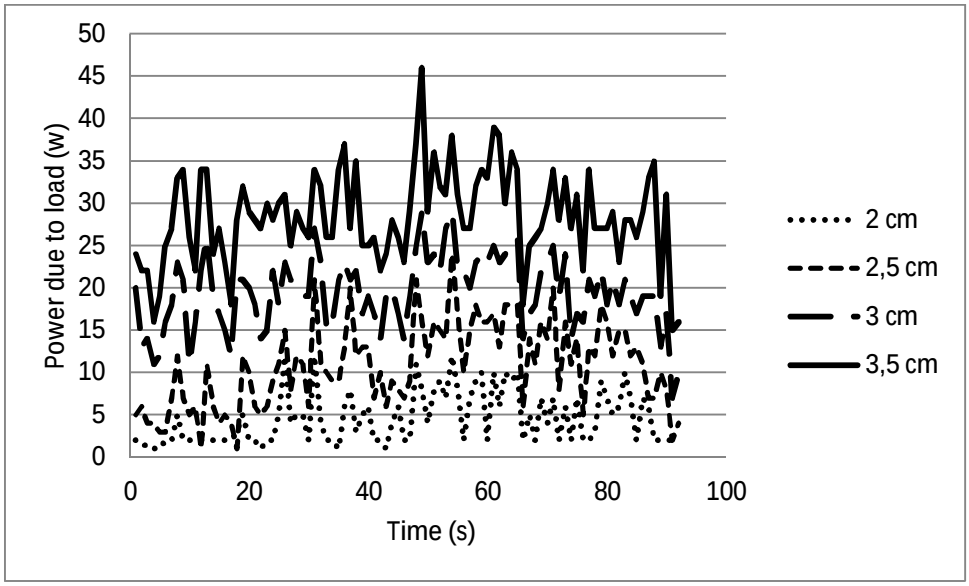

Figure 4.22 Power due to load vs time

Table 4.18 Experimental Power (Loaded) for Different Feeder Gate Heights

Feeder Gate Height	2 cm	2,5 cm	3 cm	3,5 cm
Average Power	364,2283 W	370,5543 W	374,5217 W	379,1413W
Standard Deviation	2,801504	4,312935	3,303273	3,621006

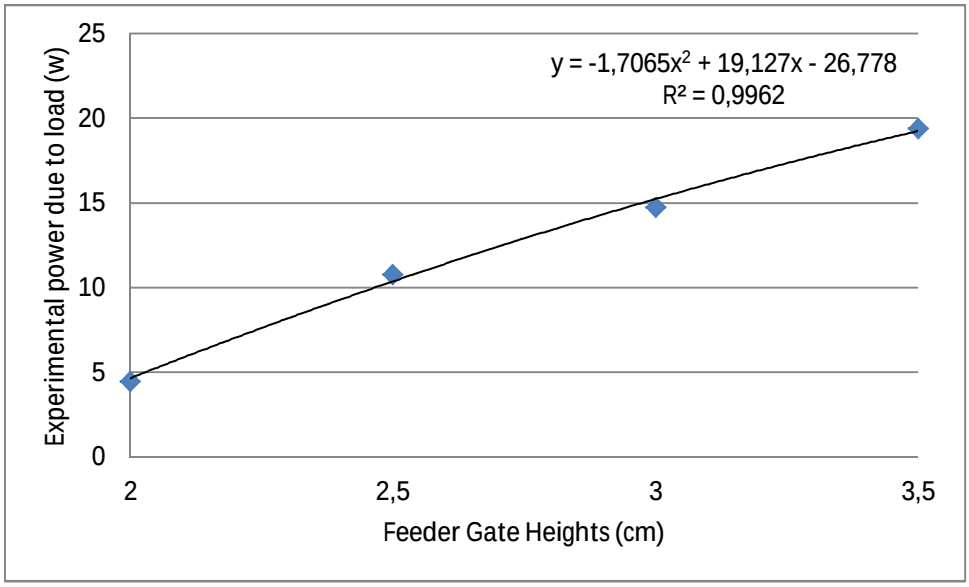

Figure 4.23 Experimental power values vs. feeder gate heights

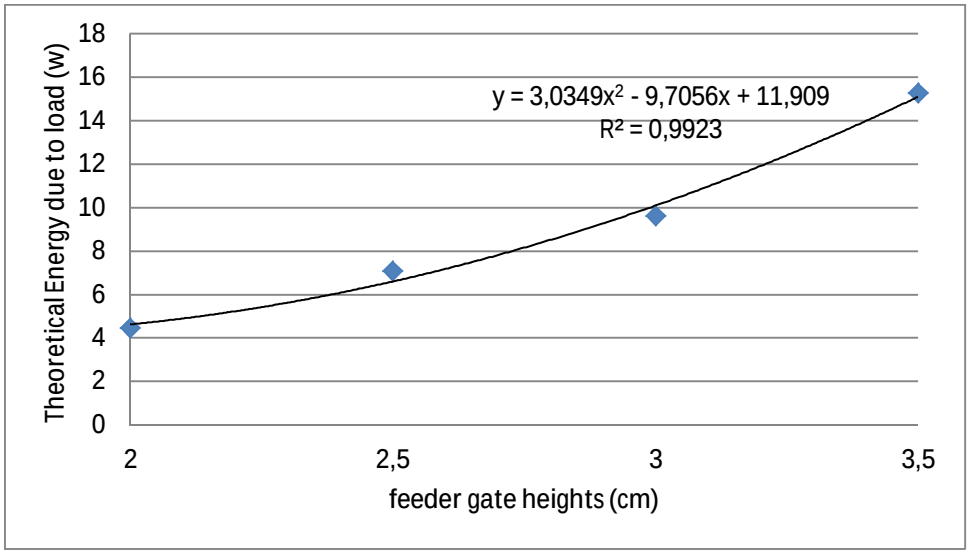

Figure 4.24 Theoretical power values vs. feeder gate heights

Table 4.19 Experimental and Theoretical (Loaded) Power Values vs Feeder Gate Height

Experiment Power Values (W)	Theoretical Power Value (W)	Feeder Gate Heights (cm)	Number of Layer
4,5	4,690688	2	1,032
10,82609	7,415398	2,5	1,304
14,79348	10,08823	3	1,584
19,41304	15,99043	3,5	2,355

4.7. Energy

There are a number of sources in the machine which requires energy at different levels. For instance, brush keeping the holes open, transmission system involving pulleys, speed reducer etc., support system such as bearings, feeder system involving cam contact, the agricultural product, are the basic sources which consume energy during the operation of system.

The total energy of the system has been explained in section 3.4.7. Unloaded energy values with or without brush against time has been plotted in Fig.4.25. Energy varies linearly with time. Brush effect can be followed from Fig 4.26 which shows peaks due to the bumps on the surface of the cylinder. Energy values due to only brush against time is presented as shown in Fig. 4.26. It is seen that without load the brush effect amounts to less than 1 %.

Under the operating conditions loaded experimental energy values are recorded against time and the resulting curves are shown in Fig 4.27. When the differences between the loaded and unloaded energy measurements for different gate heights are computed, results displayed in Fig 4.28 are obtained. As observed from Fig.4.27 the gap between the energy levels for different heights increases when the opening of the gate is changed from 2 cm to 3,5 cm. This effect is due to the increase in flow rate. The upper most value of flow rate adds about 5 % of the total energy used in the system.

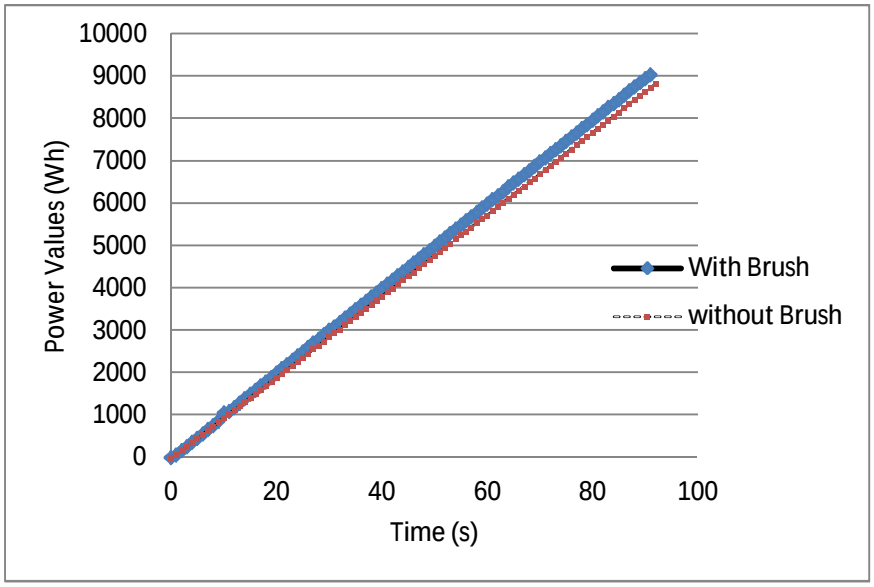

Figure 4.25 Energy values with or without brush vs time

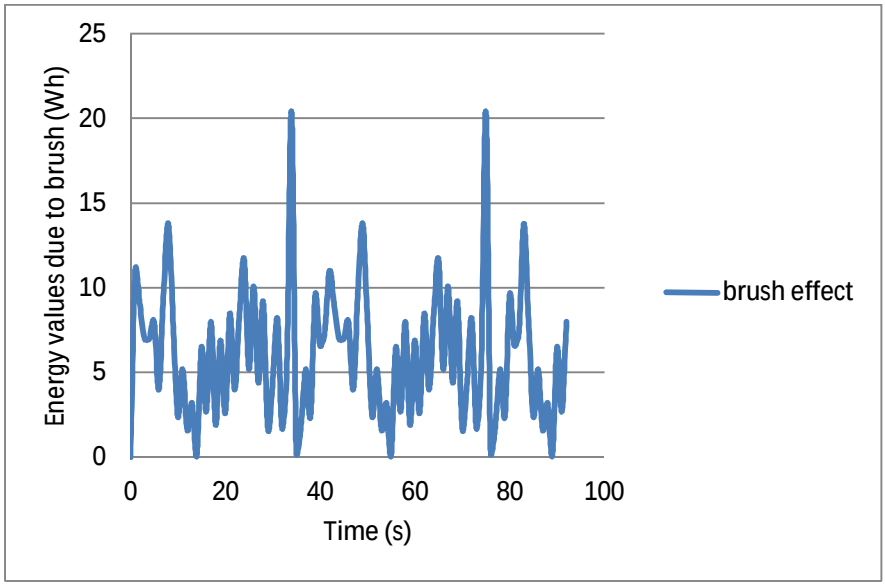

Fig. 4.26 Loaded energy values vs time

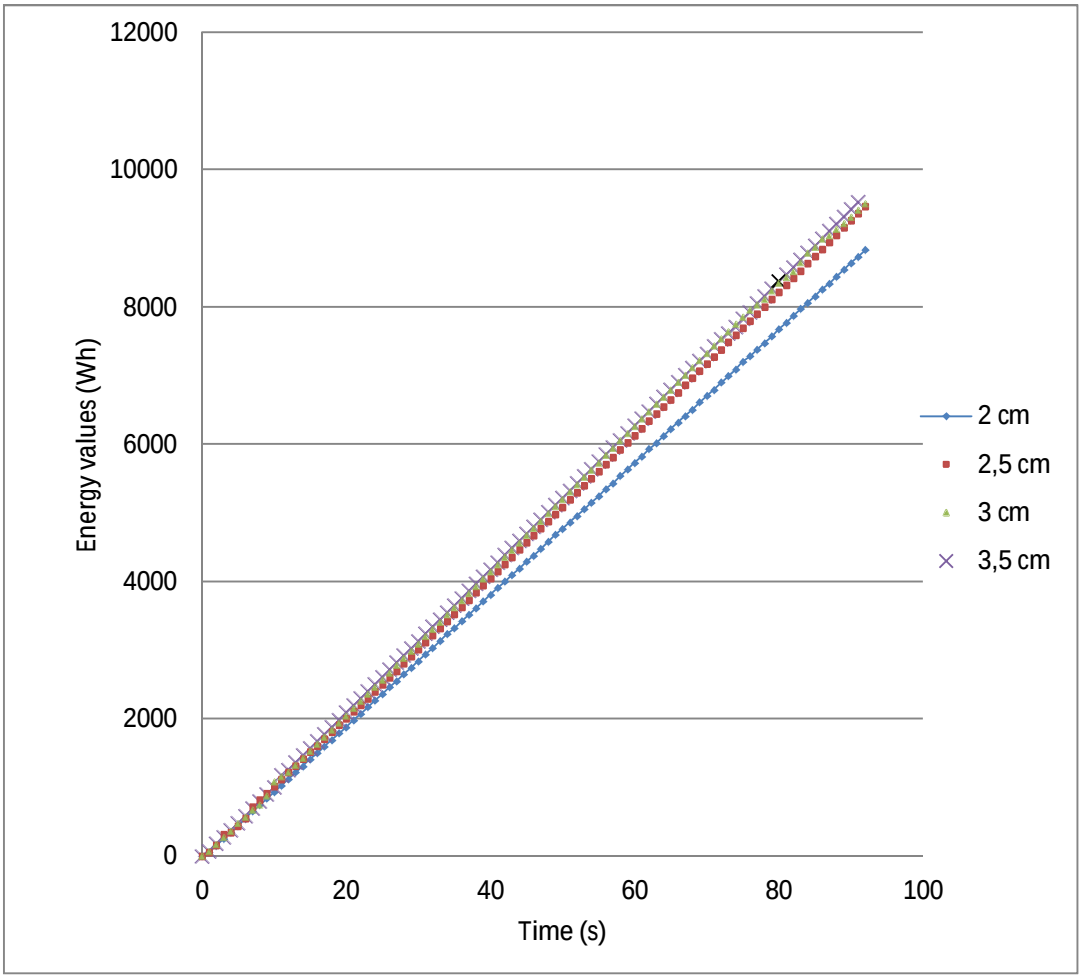

Fig. 4.27 Loaded experimental energy vs. time for different feeder gate heights

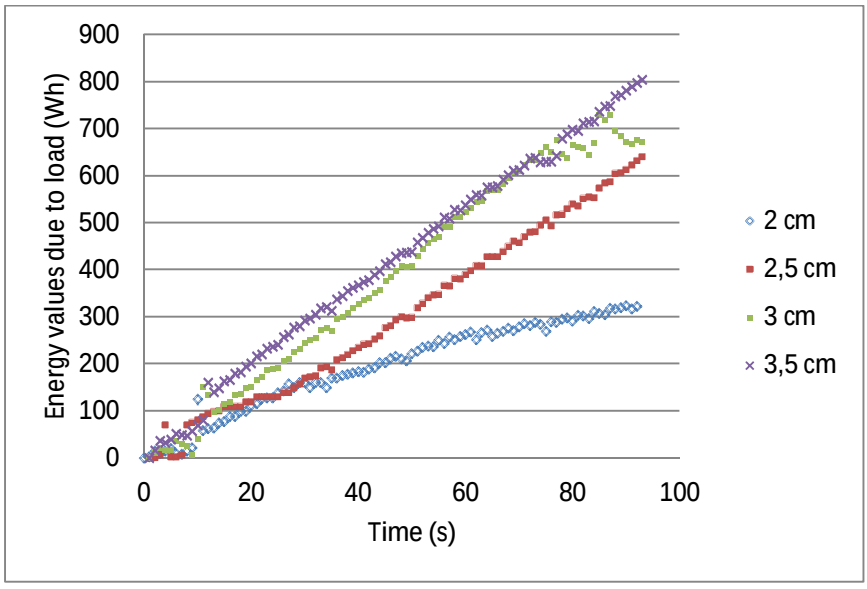

Fig. 4.28 Loaded energy values due to load vs time

5. CONCLUSION

The ultimate goal of this work is to examine the sieving function of granular material. Another goal of this study is to show the agreement between the theoretical and experimental results. As a result of the experimental and theoretical calculations, efficiency of the machine has been found to be very high and energy consumption for this purpose has turned out to be low.

Kidney bean has been used as an agricultural product to investigate the system behavior both theoretically and experimentally. In the following paragraphs all the numerical values pertain to this product.

Efficiency of sieve maximum has been found to be between 99, 86 % and 98,64 % when feeder gate height is 2 cm. Similarly, minimum efficiency is 98,0 5% to 95,25 % at the feeder gate height of 3,5 cm. Minimum feeder flow rate of the feeder is 413,17 kg/h when feeder gate height is 2 cm. Maximum feeder flow rate is 2331, 60 kg/h at the feeder gate height of 3,5 cm. When the feeder gate height is increased feeder flow rate increases. System control parameter is feeder gate. Depending on the wish to operate the system at different efficiency level, corresponding feeder gate height can be selected to satisfy certain flow rate and efficiency conditions.

When there is no load on the system (i.e. no kidney bean) in the cylinder; brushes require approximately 38 % of the driving torque applied on the machine. The highest torque value due to load has materialized as 14,22 Nm at feeder gate height of 3,5 cm . The lowest torque value has resulted as 5,22Nm, at feeder gate height of 2 cm.

Under unloaded operating conditions the average brush consumption has been found to be 9,03 W. Under loaded conditions power consumption over the given time span has turned out to be 4,5 W and 19,41 W corresponding to the feeder gate heights of 2 cm and 3,5 cm, respectively.

Energy consumption of cylindrical helical sieve within a period of 1.5 minute due to load has been found to be 9,150 kWs when feeder gate height is 2 cm. Energy consumption has increased to 9,633 kWs at a feeder gate height of 3,5 cm.

Experiments have shown that the helical sorting machine is operated under very low power consumption with very high efficiency. It is observed that brushes contribute to improve sorting function of the system. Despite some power consumption they also lead to raise the efficiency level.

If the helical cylindrical sieve is manufactured carefully and properly, sorting can be achieved with high efficiency and low energy consumption. Helical cylindrical sieve can be utilized for sorting different granular material such as peanuts, peas, soy beans etc.

In this work single and multi-layer models with linearly varying thicknesses have been considered while developing the theory of the helical cylindrical sieve. It is possible that multi layer models with non-linearly varying thickness can also be taken into account.

This system has been used alone. However, it can be proposed to operate also within an integrated system so as to include other food processes that depend on sorting function.

REFERENCES

Akcali, I.D., Ince A., & Guzel, E. (2006). *Selected physical properties of peanuts*. International journal of food properties, (9), 25–37.

Akcali, I.D., Guven, O. (1990). *Physical properties of peanut in turkey,* Agricultural mechanization in Asia, Africa, and Latin America, (3) 55-60.

Alkhaldi, H., Eberhard, P. (2006). *Computation of screening phenonema in a vertical tumbling cylinder,* Proceeding applied mathematics and mechanics, (6), 83–84.

Ata A. A., Rafeek A., Hanani Y., (2005). *Sensory-based colour sorting automated robotic cell,* Journal of Intelligent and Robotic Systems, Springer, 43, 99–110.

Brosnan, T., Sun D.W.,(2002). *Inspection and grading of agricultural and food products by computer vision systems-a review.* Computers and Electronics in Agriculture 36 , 193-213.

Brosnan, T., Sun, D.W., (2004). *Improving quality inspection of food products by computer vision—a review,* Journal of Food Engineering 61, 3–16.

Fellows, P. (2000). *Food processing technology* (2nd ed. pp.87). Cambridge, England.

Feistritzer, W.P., Vock. H., & Reiter. H.(1981). *Cereal and grain-legume seed processing* (Plant production and protection series no.21, pp. 77). Rome, Italy.

Grandison, A. S. (2006). Postharvest handling and preparation of foods for processing. Brennan J. G. (Ed.), *Food processing handbook* (pp. 21). Weinheim, Germany.

Guang-rong L., (2010) *Rice color inspection based on image processing technique.* IEEE International Conference on Advances in Energy Engineering, 134 – 137.

Guzel, E., Akcali, I.D., & Ince A. (2007). *Behavior of peanut bulk under static loads,* Journal of food engineering, (5), 385–390

Guzel, E., Akcali, I.D., Mutlu, H., & Ince, A. (2005). *Research on fatigue behavior for peanut shelling,* Journal of food engineering, (3), 373–378.

Hongchang. L., Yaoming. L. (2011). S*imulation and analysis of nonlinear motion for material particles on vibrating screen,* IEEE international conference publication on new technology of agricultural engineering (ICAE), (5), 38-43.

He, X. M., Liu C. S. (2009). *Dynamics and screening characteristics of a vibrating screen with variable elliptical trace*, Mining science and technology, (19), 0508–0513.

Narendra V. G., Hareesh K. S., (2010) *Quality inspection and grading of agricultural and food products by computer vision- a review.* International Journal of Computer Applications (0975 – 8887) Volume 2 – No.1, 43–65.

Lala, Z., Yuemin, Z., Liu Chusheng, Li Jun, & Hailin, D. (2011). S*imulation of the screening process on a circularly vibrating screen using 3d-dem*, Mining science and technology (China), (21), 677–680.

Shen, H. P., Li, J., Deng, J. M., Liu, Y. W., Ding, L., Zhang, J. T., Zhang, H. F., & Yang, T. L. (2009). *A novel vibration sieve based on the parallel mechanism*, IEEE 10th international conference publication on computer-aided industrial design & conceptual design, (4), 2328-2332.

Shuang, C., Nian-qin G.,(2010). Optimization of super-heavy vibrating screen based on MATLAB , IEEE 3rd International Conference on Information and Computing,(3), 262 – 264.

Steyn J., (1995). *Fatigue failure of deck support beams on a vibrating screen*. J. Pres. Vex & Piping, 61, 315-327.

Stoicovici, D. I., Ungureanu M., Ungureanu, N., & Banica M. (2009). *Computer model for sieves' vibrations analysis, using an algorithm based on the false-position method*, American journal of applied sciences, (6) , 48-56.

Ronghua S.,, Liuqing Z.,, Chenyu P., (2010). CAE Applied to dynamic optimal design for large-scale vibrating screen, IEEE 2010 First ACIS International Symposium on Cryptography, and Network Security, Data Mining and Knowledge Discovery, E-Commerce and Its Applications, and Embedded Systems, 316 – 320.

Tan, J., Harrison H. P. (1987). *Screening efficiency for planar and spatial drive mechanisms*, American society of agricultural engineers, 30(5), 1242-1253.

Unay, D., Gosselin, B., (2004). *A qualıty sortıng method for 'jonagold' apples*, Engineering the Future (International Conference of Agricultural Engineering) 12-16 September 2004, Leuven, Belgium.

Yan, J., Liu, C., Zhao, L., Li, J., (2010). *Parameters optimum design for linear vibrating screen*, IEEE International Conference on Computational and Information Sciences, 413 – 415.

Yue-m, Z., Chu-sheng, L., Xiao-mei, H., Cheng-yong, Z., Yi-bin, W., Zi-ting, R., (2009). *Dynamic design theory and application of large vibrating screen* .The 6th International Conference on Mining Science & Technology, 2009 Published by Elsevier Procedia Earth and Planetary Science 1 , 776–784 .

Zhongjun, Y., Tian, H., Xin,S., Lianwan, Z., *Research on dynamic characteristics of elliptical vibrating screen*, IEEE International Conference on Mechanic Automation and Control Engineering (MACE), 2366 – 2369.

http://www.compacsort.com/wawcs0114832/idDetails=112/Internal/Taste%28N.I.R%29.html (last access: 30.06.2012)

BIOGRAPHY

Umut ERCAN was born on July 08, 1983 in Adana, Turkey. He graduated from High School In 2000, and enrolled at Fırat University to study mechanical engineering. He graduated with a Bachelor of Science degree in mechanical engineering from the Department of Mechanical Engineering in 2008. He began his MSc studies at the Department of Mechanical Engineering of Çukurova University in 2008. He worked in İNSPEGO International Inspection & Certification Services Ltd. 2011 and 2012. He has been working as Research Assistant in the Automotive Engineering Department of Batman University since February, 2012.